frontiers | Frontiers in Materials

TYPE Original Research
PUBLISHED 13 October 2023
DOI 10.3389/fmats.2023.1272869

OPEN ACCESS

EDITED BY
Noemi Orazi,
University of Rome Tor Vergata, Italy

REVIEWED BY
Qaisar Maqbool,
Marche Polytechnic University, Italy
Gomaa Abdel-Maksoud,
Cairo University, Egypt

*CORRESPONDENCE
Ioana Cristina Marinas,
ioana.cristina.marinas@gmail.com

†These authors have contributed equally to this work

RECEIVED 04 August 2023
ACCEPTED 15 September 2023
PUBLISHED 13 October 2023

CITATION
Corbu VM, Dumbravă AŞ, Marinescu L, Motelica L, Chircov C, Surdu AV, Gheorghe-Barbu I, Pecete I, Balotescu I, Popa M, Marinas IC, Ianovici N, Ciobanu D-G, Dițu LM, Ficai D, Oprea OC, Ficai A, Eugenia Șesan T and Chifiriuc MC (2023), Alternative mitigating solutions based on inorganic nanoparticles for the preservation of cultural heritage. *Front. Mater.* 10:1272869. doi: 10.3389/fmats.2023.1272869

Alternative mitigating solutions based on inorganic nanoparticles for the preservation of cultural heritage

Viorica Maria Corbu[1,2†], Andreea Ştefania Dumbravă[3,4], Liliana Marinescu[5], Ludmila Motelica[5,6], Cristina Chircov[5,6], Adrian Vasile Surdu[5,6], Irina Gheorghe-Barbu[1,3†], Ionuț Pecete[7], Irina Balotescu[1], Marcela Popa[1], Ioana Cristina Marinas[1]*, Nicoleta Ianovici[8], Daniela-Georgiana Ciobanu[8], Lia Mara Dițu[1,3], Denisa Ficai[9], Ovidiu Cristian Oprea[6,9,10], Anton Ficai[5,6,10], Tatiana Eugenia Șesan[3,11] and Mariana Carmen Chifiriuc[1,3,10,12]

[1]Research Institute of the University of Bucharest, University of Bucharest, Bucharest, Romania, [2]Department of Genetics, Faculty of Biology, University of Bucharest, Bucharest, Romania, [3]Department of Microbiology and Botany, Faculty of Biology, University of Bucharest, Bucharest, Romania, [4]Department of Technological Irradiation (IRASM), Horia Hulubei National Institute of Physics and Nuclear Engineering–IFIN-HH, Măgurele, Romania, [5]Department of Science and Engineering of Oxide Materials and Nanomaterials, Faculty of Chemical Engineering and Biotechnologies, University POLITEHNICA of Bucharest, Bucharest, Romania, [6]National Centre for Micro and Nanomaterials and National Centre for Food Safety, University POLITEHNICA of Bucharest, Bucharest, Romania, [7]Central Reference Synevo-Medicover Laboratory, Bucharest, Romania, [8]Department of Biology-Chemistry, Environmental Biology and Biomonitoring Research Center, West University of Timisoara, Timișoara, Romania, [9]Department of Inorganic Chemistry, Physical Chemistry and Electrochemistry, Faculty of Chemical Engineering and Biotechnologies, University POLITEHNICA of Bucharest, Bucharest, Romania, [10]Academy of Romanian Scientist, Bucharest, Romania, [11]Romanian Academy of Agricultural and Forestry Sciences, Bucharest, Romania, [12]Romanian Academy, Bucharest, Romania

Introduction: Biodeterioration is a big challenge for the preservation of cultural heritage objects and for the community's safety, fostering the search for novel methods effective in removing microbial biofilms and subsequent biodeterioration. In this context, nanoparticles (NPs) are considered an interesting alternative, based on their unique physico-chemical and biological properties.

Methods: The present study aimed to evaluate the antimicrobial efficiency of Ag, Au, Cu, and ZnO NPs against a significant number of filamentous fungi and bacterial strains isolated from wooden and stone cultural heritage objects from different Romanian regions, as well as from museum collections, with the final goal to establish their potential to develop novel preservation strategies, which have high efficiency and low ecotoxicity.

Results: Six types of nanoparticles (NPs) based on Ag, Au, Cu, and ZnO were synthesized and characterized for their physico-chemical properties, ecotoxicity, and efficacy against 75 filamentous fungi and 17 bacterial strains isolated from wooden and stone cultural heritage objects (15th–19th century). The results showed that all synthetized NPs are homogeneous, demonstrating a good stabilizing coating, and have spherical or triangular shapes, with sizes between 9 and 25 nm. The highest antifungal efficiency has been recorded for Ag NPs, followed by Cu NPs and ZnO NPs, with the most susceptible strains being *Aspergillus montevidensis*, *Penicillium commune*, *Penicillium corylophilum*, *Bacillus megaterium*, and *B. cereus*. The Cu NPs and ZnO NPs decreased the

capacity of microbial strains to adhere to the inert substratum. The influence of the tested NPs against enzyme/organic acid production varied depending on the NP types and by species.

Conclusion: The obtained results are promising for the development of efficient and economical alternative solutions for heritage preservation, showing high antimicrobial activity against the prevalent fungal and bacterial strains involved in the biodeterioration of Romanian heritage objects.

KEYWORDS

cultural heritage objects, biodeterioration, enzyme/organic acid production, nanoparticles, antimicrobial activity, antibiofilm activity, ecotoxicity

1 Introduction

The cultural heritage of each country represents a bridge between its past, present, and future, not only being a testimony of the way in which human civilization has evolved but also an important source of income for the national economy by capitalizing on the tourism potential. The physical, chemical, and biological degradation of cultural heritage objects represents a real societal challenge, leading to both cultural and economic loss (P. et al., 2018). Biodeterioration can be caused by macro-organisms such as lichens, plant mosses, plants or insects, and various microorganisms (including bacteria, archaea, fungi, and microalgae), which are directly responsible for altering the appearance and integrity of different materials such as paper, leather, textiles, wood, glass, or stone due to their versatile metabolism (Carpino et al., 2023). The objects may be fully damaged and lost if the biodegradation process is not stopped in time. Due to the activity of certain enzymes (cellulases, proteases, and collagenases) and organic acids, materials based on cellulose and collagen are especially vulnerable to fungal and bacterial degradation under certain circumstances (Bella et al., 2015).

Among the microorganisms responsible for deterioration, fungi are more likely to be identified. They belong to two major categories: a) opportunistic fungi, that can colonize nearly any material in a properly humid environment but are unable to depolymerize the materials' structural components and b) cellulolytic and keratinolytic fungi, which have specific enzymatic abilities to break down various polymers (leather, hair, and feathers—keratinolytic; wood, paper, and parchment—cellulolytic) and to alter the object structure. Amid the most prevalent deteriogenic fungal genera are different species of *Penicillium*, *Cladosporium, Alternaria, Aspergillus, Chrysosporium, Fusarium, Geotrichum,* and *Paecilomyces* (Sterflinger and Pinzari, 2012). Among bacteria, the most often isolated species from cultural heritage items are heterotrophic bacteria, belonging to *Bacillus, Micrococcus, Staphylococcus, Paenibacillus, Flavobacterium, Pseudomonas, Nocardia, Mycobacterium,* and *Streptomyces* genera. In general, they express a variety of enzymes, such as cellulases, keratinases, and esterases, active in the degradation of textiles (*Bacillus* spp.), or lipases, amylases, proteases, having solventogenic activity, involved in the degradation of paintings and icons (*Pseudomonas* spp.) (Sterflinger and Piñar, 2013; Pyzik et al., 2021).

Disinfection is the most efficient method to prevent biodeterioration, the most used chemical agents being quaternary ammonium salts, ethylene oxide, alcohols, aldehydes, halogen compounds, dyes, peroxides, surfactants, and heavy metals (like silver, copper, and gold). Ethylene oxide is the most popular method for sanitizing historical artifacts; its exceptional efficacy is unmatched by any other fumigant. Unfortunately, the gas is mutagenic, carcinogenic, and causes allergic responses in addition to irritating the respiratory system (Pietrzak et al., 2016). Since mechanical methods may cause prejudices to fragile cultural heritage objects, and chemical methods may contribute negatively to pollution, new strategies to prevent their deterioration are urgently needed. Nanotechnology has shown significant potential in the field of preservation, offering novel instruments and techniques to achieve higher consolidation and safeguarding efficiency. Due to their small particle size, nanomaterials (NMs) (1–100 nm) may be able to penetrate deeper into damaged artifacts compared to larger-scale materials (S. et al., 2018). In recent years, inorganic nanoparticles (NPs) (Cu, Au, Ag, TiO_2, ZnO, SiO_2, and CuO) have been used for strengthening various artifacts and artworks (Blee and Matisons, 2008; Ion et al., 2018; David et al., 2020) and also for protecting the surfaces of various buildings against biofilm formation, acting by assuring surface self-cleaning, by improving the surface of the material, or by exhibiting biocidal activity (Reves-Estebanez et al., 2018). Due to their small particle size, NPs may be able to penetrate deeper into damaged artifacts compared to larger-scale materials (Mourdikoudis et al., 2018).

Oxide materials such as TiO_2 and SiO_2 have been successfully used in the process of strengthening ceramic artifacts, forming a transparent, uniform, and hydrophobic layer on the artifacts' surface; moreover, the NPs penetrated the surface of the artifacts, providing them with a greater resistance, without inducing any chemical, physical, or aesthetic changes (Barberio et al., 2015). The performance of Ag, Cu, ZnO, and TiO_2 NPs has been studied for their anti-termite, rot, mold, fungal, and UV degradation activity, with the results showing that these NPs have significantly improved the resistance and prevented the degradation of wooden artifacts.

The MgO NPs inhibited the fungal contamination of paper objects, particularly with *Aspergillus niger*, *Cladosporium cladosporioides*, and *Trichodernma reesei* strains, without affecting the paper quality (Castillo et al. (2019). The MgO NPs inhibited the cellulase production in *T. reesei* and *A. niger*, two of the main deteriogenic agents of cellulosic materials (Castillo et al., 2019). There are various additional studies on the use of Ag NPs applied to cotton textiles for antibacterial finishing or of ZnO NPs to inhibit fungal biofilms (Balakumaran et al., 2016; Gambino et al., 2017). Moreover, Ag NPs alter the formation and morphology of the mycelium, affecting

the development and germination of conidia as well as the pigmentation of *Penicillium brevicompactum*, *Aspergillus fumigatus*, *C. cladosporioides, Stachybotrys chartarum*, and *Chaetomium globosum* conidiophores and conidia (Ogar et al., 2015). CuO NPs and different plant extracts (*Azadirachta indica*, *Pongamia pinnata*, *Lantana camara*, and *Citrus reticulata*) have shown the capacity to cure and preserve wood degraded by deteriogenic bacteria and by the activity of termites (Shiny et al., 2019). A study conducted by Fouda et al. in 2019 proved that Ag NPs and ZnO NPs are efficient for paper preservation (Zhang et al., 2016). Motelica et al. (2021) have shown that ZnO NPs can be successfully used to protect manual paper from old books, removing the pathogens and preventing any further growth. ZnO NPs are intensively studied for outdoor antimicrobial applications since this type of NPs is characterized by high stability and corrosion resistance when they are exposed to different environmental conditions (Abdel-Daim et al., 2019). Due to their antibacterial and antibiofilm activity, Au NPs in association with hydroxyapatite (HAp) proved to improve the structure of hazel wood (Ion et al., 2018).

Very few studies have been carried out in Romania regarding the antimicrobial efficiency of alternative solutions against deteriogenic microorganisms of tangible cultural heritage (Fierascu et al., 2014; Corbu et al., 2021, 2022; Gheorghe et al., 2021; Ilies et al., 2021). The wooden and stone churches from the 14 to 19 centuries are a recognizable representation of Romanian national history, serving as significant locations for the founding communities' secular as well as spiritual individual and communal gatherings (Gheorghe et al., 2021). The purpose of the current study was to demonstrate the antimicrobial efficiency of several metal and metal oxide nanoparticles (Ag, Au, Cu, and ZnO NPs) against a significant number of filamentous fungi and bacterial strains isolated from wooden and stone cultural heritage objects, for further developing novel preservation strategies, with good efficiency and low ecotoxicity, adapted to the characteristics of tangible heritage objects.

2 Materials and methods

2.1 Materials

Zinc acetate dihydrate ($Zn(CH_3COO)_2{\cdot}2H_2O$), 99.9% was purchased from Merck. Silver nitrate ($AgNO_3$), sodium borohydride ($NaBH_4$), copper (II) sulfate ($CuSO_4{\cdot}5H_2O$), sodium hydroxide (NaOH), and gold (III) trichloride ($AuCl_3$) were purchased from Sigma Aldrich; polyvinylpyrrolidone (PVP), hydrazine (N_2H_4), L-ascorbic acid ($HC_6H_7O_6$), and polyethylene glycol (PEG 400) from Roth; hydrogen peroxide (30% H_2O_2) from Silal Trading; lecithin ($C_{42}H_{80}NO_8P$) and trisodium citrate ($Na_3C_6H_5O_7$) from Alfa Aesar; and 1-butanol from Merck. All reagents and solvents were used without further purification.

2.2 Methods

2.2.1 Synthesis of Ag NPs

2.2.1.1 Synthesis of Ag NPs by the classical method, at room temperature (Ag NPc)

Approximately 500 ml of 0.0001 M $AgNO_3$ solution was introduced into a Berzelius beaker, then 30 ml of 0.02999 M trisodium citrate was added. The solution thus obtained was left under continuous agitation (600–700 rpm) for 12 min, at room temperature. After 12 min, 30 ml of 0.00007 M PVP was added. The solution was stirred for 1 min (200 rpm), after which 3 ml of 0.1 M sodium borohydride solution was added. The final mixture was stirred for 5–7 min, after which 1.2 ml of 30% hydrogen peroxide was added. After adding H_2O_2, the obtained solution was stirred until a blue or emerald blue color appeared. The concentration of the obtained NPs was 10 ppm.

2.2.1.2 Synthesis of Ag NPs by the Turkevich method (Ag NPt)

Approximately 0.01 g of $AgNO_3$ was dissolved in 500 mL of H_2O. The obtained solution was kept at 70°C–75°C under magnetic stirring for 75 min. To this solution, a solution containing 0.30 g of sodium salt of citric acid was added dropwise, which acted as the reducing agent. When the solution became slightly yellowish, 10 mL of PVP was added. The concentration of the obtained NPs was 100 ppm.

2.2.1.3 Synthesis of Ag NPs by the hydrothermal method (Ag NPsol)

Approximately 0.888 g of PVP K 30 was added to 80 mL of PEG 400. The mixture was stirred and heated to 80°C until the obtained solution became transparent. When the temperature reached 80°C, 2 mL of $AgNO_3$ with a concentration of 0.5 M was quickly added to the mixture, under stirring. A dark yellow color was observed, and the mixing was continued at 80°C until the appearance of a dark brown color. The mixture was poured into a Teflon vat, and the temperature was increased to 220°C while maintaining a constant pressure of 1 bar for 2 h. The reddish-brown mixture was cooled and then removed from the vat. The concentration of the obtained NPs was 1,000 ppm.

2.2.2 Synthesis of ZnO NPs

ZnO NPs were prepared using the solvothermal method described in Motelica et al. (2021). Briefly, 5.000 g of $Zn(Ac)_2{\cdot}2H_2O$ was mixed with 50 ml of 1-butanol and refluxed at boiling point for 48 h. After the reflux time, the flask was removed from the heater and allowed to rest for another 24 h at room temperature. The obtained white precipitate was centrifuged at 9,000 rpm, washed three times with C_2H_5OH, and dried in an electrical oven at 105°C. ZnO NPs with an average size of ~20 nm were obtained.

2.2.3 Synthesis of Cu NPs by the hydrothermal method

In a Berzelius glass, an amount of 20 g of $CuSO_4{\cdot}5H_2O$ was dissolved in 200 ml of distilled water. The obtained mixture was heated on a hot plate at 60°C for 10 min. After heating, a solution of 0.2 g of NaOH (0.5 M) in 20 ml of distilled water was added to the aforementioned mixture, with the appearance of a black precipitate. Afterward, hydrazine (70 ml) was added dropwise, maintaining the temperature, and stirring was continued for another 30 min. After the addition of hydrazine, the color changed to brown. After this treatment, the recovered/formed Cu NPs (cooled) were purified by washing them twice with distilled water and ethanol and then dried at 60°C for 2 h.

2.2.4 Synthesis of Au NPs by the hydrothermal method

The synthesis of Au NPs was carried out according to the literature with slight modifications (Aziz et al., 2017). An aqueous solution of gold salt ($AuCl_3$, 30 mL, 1 mM) was added in a Berzelius beaker and maintained at 50°C under stirring, and then an aqueous solution of lecithin (4.5 mL, 20 mM) was added. Then, l-ascorbic acid (0.75 mL, 100 mM) was added under continuous stirring. Finally, trisodium citrate (0.75 mL, 100 mM) was added to this solution and stirred for 2 h at 50°C. The AuNP colloidal solution was centrifuged at 7,000 rpm for 15 min. The settled particles were collected and dispersed in water. The purification process was repeated three times with deionized water.

2.2.5 NP characterization

The NPs obtained were characterized by specific physico-chemical methods: X-ray diffraction (XRD), infrared spectroscopy (FTIR), dynamic light scattering (DLS), scanning electron microscopy (SEM), and UV–Vis spectroscopy. X-ray diffraction patterns (XRD) were recorded on a PANalytical X'Pert Pro MPD analyzer using Cu-K radiation; IR spectroscopy measurements were performed using a Thermo Nicolet™ iS50 FTIR spectrometer equipped with a diamond crystal-based ATR module capable of recording spectra over a range of 400–4,000 cm^{-1}. To obtain a better signal-to-noise ratio, the spectra were obtained by summing 16 scans recorded at a resolution of 8 cm^{-1}. The acquisition time was set to 3 scans/s using a DTGS type detector and an automatic beam splitter (beam splitter) for the ability to record the spectrum, especially in the transmission mode, in the range 10–25,000 cm^{-1}, i.e., from far IR to near IR. The DLS measurements were carried out using a DelsaMax PRO light scattering analyzer, with reusable PEEK flow cells, BCI-3216-DMP, and a DLS detector angle (degree) of 163.5°. The acquisition parameters for this technique were as follows: acquisition time(s): 5 s acquisition time, 1 s read interval, with a 15-s collection period for three acquisitions, at 10 Hz electric field frequency, with auto-attenuation set at 0% level, normal laser mode, with the temperature set at 20°C. SEM images were recorded using a Quanta Inspect F; FEI microscope equipped with an EDS spectrometer, the samples being covered with a thin film of silver. A JASCO (Easton, PA, United States) V-560 spectrophotometer equipped with a 60-mm integrating sphere (ISV-469) was used to record the diffuse reflectance spectra (UV–Vis). All the measurements were made in the domain 200–900 nm, with a speed of 200 nm min^{-1}.

2.2.6 Evaluation of antimicrobial activity against the deteriogenic microbial strains

2.2.6.1 Microbial strains

The antimicrobial activity of the synthesized NPs was tested against a total of 75 filamentous fungi belonging to *Aspergillus* spp. (seven *A. niger*, five *Aspergillus* spp., three *A. sydowii*, two *A. versicolor*, *two A. pseudoglaucus*, two *A. flavus*, one *A. terreus,* one *A. nidulans*, one *A. ustus*, and one *A. montevidensis*), *Penicillium* spp. (17 *Penicillium chrysogenum*, 11 *P. corylophilum*, four *Penicillium expansum*, three *Penicillium* spp., two *P. digitatum*, two *P. nalgiovense*, two *P. commune*, one *P. italicum*, and one *P. glabratum*), *Purpureocillium lilacinum* (two), *Fusarium incarnatum* (two), *Trichoderma longibrachiatum* (one), *Mucor circinelloides* (one), and *Alternaria alternata* (one) and 17 bacterial strains belonging to *Bacillus* spp. (eight *Bacillus megaterium*, four *B. pumilus*, two *Bacillus* spp., one *B. subtilis*, one *B. cereus*, and one *B. atrophaeus*) isolated from wooden (Troas, Savarsin; Barzava, Grosii Noi; Julita, Arad; Lunca Motilor, Hunedoara; St. Hierarch Nicolae, Bucharest; and Dragoș Vodă" Putna, Suceava) and stone cultural heritage churches/monasteries (Ostrov; Orlea; Prislop Monastery, Silvasu de Sus; Paros; Densus; Nucsoara; and Sinpetru, Hunedoara; Arbore; Sfântu Ilie; Sucevița Monastery; Moldovita Monastery, and St. Ioan cel Nou, Suceava), as well as paper objects, textiles (linen, cotton, hemp, wool, etc.), wood, and ceramics from the Romanian Peasant Museum in Bucharest and the Museum of History and Archeology in Tulcea. The selection criteria for the churches were represented by age (14–19 centuries); diversity of construction materials, i.e., wood (oak wood, beech wood, softwood, pinewood, mural paintings in oak wood, etc.); stone (mountain rock, construction gravel, mural Byzantine painting, etc.); and textiles (linen, cotton, hemp, wool, etc.). Regarding the investigated churches, with the exception of St. Hierarch Nicolae from Bucharest, all wooden churches belonged to class A cultural heritage monuments of national importance, while the stone churches were included in the class B of local importance, the majority being in an advanced stage of deterioration and requiring restoration work (Gheorghe et al., 2020).

The selected buildings and objects were damaged by several physical, chemical, and biological factors (such as temperature and humidity fluctuation between different seasons, natural or artificial lighting, surface erosion or granular breakdown, black crusts, salt crystallization cycles, hygroscopic absorption, and micro- and macro-organism activity), with the effects being profound and irreversible (Gheorghe et al., 2020; Bogdan et al., 2022). The average values of relative humidity for all churches were between 67% and 79%. At the time of sampling, the temperature varied between 21°C and 27°C. An area of approximately 10 cm^2 of the discolored, altered walls of the narthex, nave, and altar and the surface of museum object samples were sampled by swabbing, followed by swab submersion in sterile distilled water, ten-fold serial dilutions, and inoculation onto three different culture media: PDA (potato dextrose agar) supplemented with chloramphenicol (0.05 g/L), Rose Bengal, and SDA (Sabouraud dextrose agar), incubated at 22°C ± 1°C for 5–7 days. The microbial strains were identified by classical methods and taxonomically confirmed by MALDI-TOF mass spectrometry.

2.2.6.2 Qualitative antimicrobial activity

The qualitative screening of the antimicrobial activity was performed by an adapted diffusion method on Sabouraud agar (SDA) for fungal strains and Mueller–Hinton agar medium for bacteria. Standard fungal cell and bacterial suspensions (1 and 0.5 McFarland) were prepared using fresh cultures of fungi (5–7 days of growth at room temperature on SDA media) and bacterial strains (24 h bacterial culture cultivated on plate count agar medium). Each suspension was evenly spread on agarized culture media, and 10 µL of each NP solution was spotted over. The plates were incubated for 5–7 days at room temperature for fungi and for 24 h at 37°C for bacterial strains. At the end of the incubation time, the growth inhibition diameter zone was measured,

and the values were converted into arbitrary units using the following convention: 0 value for no inhibition zone, 1 for a growth inhibition diameter zone up to 10 mm, and 2 for a growth inhibition diameter zone of 11–20 mm.

2.2.6.3 Quantitative antimicrobial activity

All strains for which positive results were recorded after the qualitative screening of the antimicrobial activity were used for the quantitative evaluation of the antifungal and antibacterial activity. Quantitative determination was performed using the microdilution method in 96-well (multi-well) plates. The serial two-fold microdilutions of the compounds were achieved in 100 µL of RPMI (Roswell Park Memorial Institute) 1640 medium for fungi and Mueller–Hinton broth for bacteria, and each well was subsequently inoculated with 10 µL of microbial suspensions made according to the protocol described for qualitative testing. After 5–7 days of incubation at room temperature (for fungi) and 24 h at 37°C (for bacteria), the microbial growth and multiplication were determined spectrophotometrically by monitoring the optical density at 600 nm. The minimum inhibitory concentration (MIC) values were established in correspondence to the lowest concentration, at which the tested plant extract inhibited the multiplication of the microbial cultures.

2.2.7 The influence of NPs on the microbial adherence capacity to the inert substratum

To determine the influence of the tested NPs to inhibit microbial adherence to the inert substratum (96-well plate, untreated polystyrene), the crystal violet microtiter method was used. Each microbial strain was cultivated in the presence of MIC/2 concentrations of the tested NPs, and after 5 days in the case of fungi and 24 h for bacteria, the adhered cells were fixed using methanol and stained with 1% crystal violet solution. After staining, the adhered cells were resuspended in 33% acetic acid solution and quantified by measuring the absorbance at 490 nm. Appropriate negative and positive controls were used to determine the influence of the NPs on microbial adherence. The formula used for the evaluation of the microbial adherence capacity was IIBG% = 100 − (ANp × 100)/Ac, where ANp = the absorbance of the biofilm formed and treated with a sub-inhibitory concentration of NPs and Ac = the absorbance of the biofilm formed untreated.

2.2.8 The influence of NPs on metabolic activity

Selected microbial strains (both fungi and bacteria) able to produce and secrete biodegradative enzymes such as cellulase, esterase, amylase, and caseinase, as well as organic acids, were used for determining the influence of the NP solution at sub-inhibitory concentrations on their metabolic activity. Each strain was cultivated in the presence of sub-inhibitory concentration of NP solutions (MIC/2) for 7 days in the case of fungi and 24 h for bacteria, and subsequently, 1 McFarland standard suspensions were prepared in sterile 0.7% sodium chloride solution. Each specific culture medium (Corbu et al., 2022) was spotted with 10 µL of treated and untreated microbial suspensions and then incubated at 26°C–28°C for 5–8 days in the case of fungi and 24 h for bacterial strains. The NP solution's impact on the metabolic profile was semi-quantitatively evaluated by measuring the ratio of the colony diameter (C) to the diameter of the specific inhibition zone occurring around the colony (D) and then applying the following formula:

$$\text{Inhibition}\,(\%) = (D2 - C2) \times 100/(D1 - C1),$$

where C1—colony diameter of the control strain, D1—inhibitory effect zone diameter of strain control, C2—colony diameter of the treated strain, and D2—inhibitory effect zone diameter of the treated strain.

2.2.9 Ecotoxicity of NPs

The ecotoxicity of the tested NP solutions was investigated using the *Allium* assay (Datcu et al., 2020). Thus, bulbs of *Allium cepa* var *rubra* selected based on macroscopic observation of morphological characteristics and integrity were used. These were divided into six sets. The healthy bulbs were maintained in tap water for 6 days to form roots at room temperature. A set of control samples were introduced into distilled water. An equal volume of NP was added, and the bulbs were analyzed after 24 h of contact. For the fresh biomass determination, the bulbs were weighted using an analytical balance. The daily weight gain of the bulbs was calculated for the pre-test (before adding the tested solutions) and post-test (after 24 h of contact) periods. The differences were evaluated with the *t*-test ($p < 0.05$).

2.2.10 Statistical analysis

Data were expressed as mean ± SD, and statistical analysis was performed using GraphPad Prism v9. Data were analyzed using ordinary two-way ANOVA using *post hoc* tests (Sidak's correction) for multiple comparisons, with individual variances calculated for comparison between the biological activities of NPs and the control strain. In the case of ecotoxicity, the differences were evaluated with the unpaired *t*-test by the Holm–Sidak method for comparison between the pre-test (before adding the tested solutions) and post-test period (after 24 h of contact). The significance level was set at $p < 0.05$.

3 Results

3.1 The obtaining and characterization of the NPs

Six types of NPs were synthesized: Ag NPs by the classical method (Ag NPc), Ag NPs by the Turkevich method (Ag NPt), Ag NPs by the hydrothermal method (Ag NPsol), Cu NPs, ZnO NPs, and Au NPs. The obtained NPs were characterized by XRD, FTIR, DLS, SEM, and UV–Vis methods.

3.1.1 XRD

The formation of the zinc oxide phase using the solvothermal method was confirmed using an X-ray diffractogram. X-ray diffraction was used to establish the formation of ZnO NPs as a pure phase. The recorded X-ray diffractograms (Figure 1A) indicate the presence of ZnO NPs as a single phase. In the XRD diffractograms, the characteristic peaks of the Wurtzite-type hexagonal structure ZnO NPs can be observed at the 2θ angle

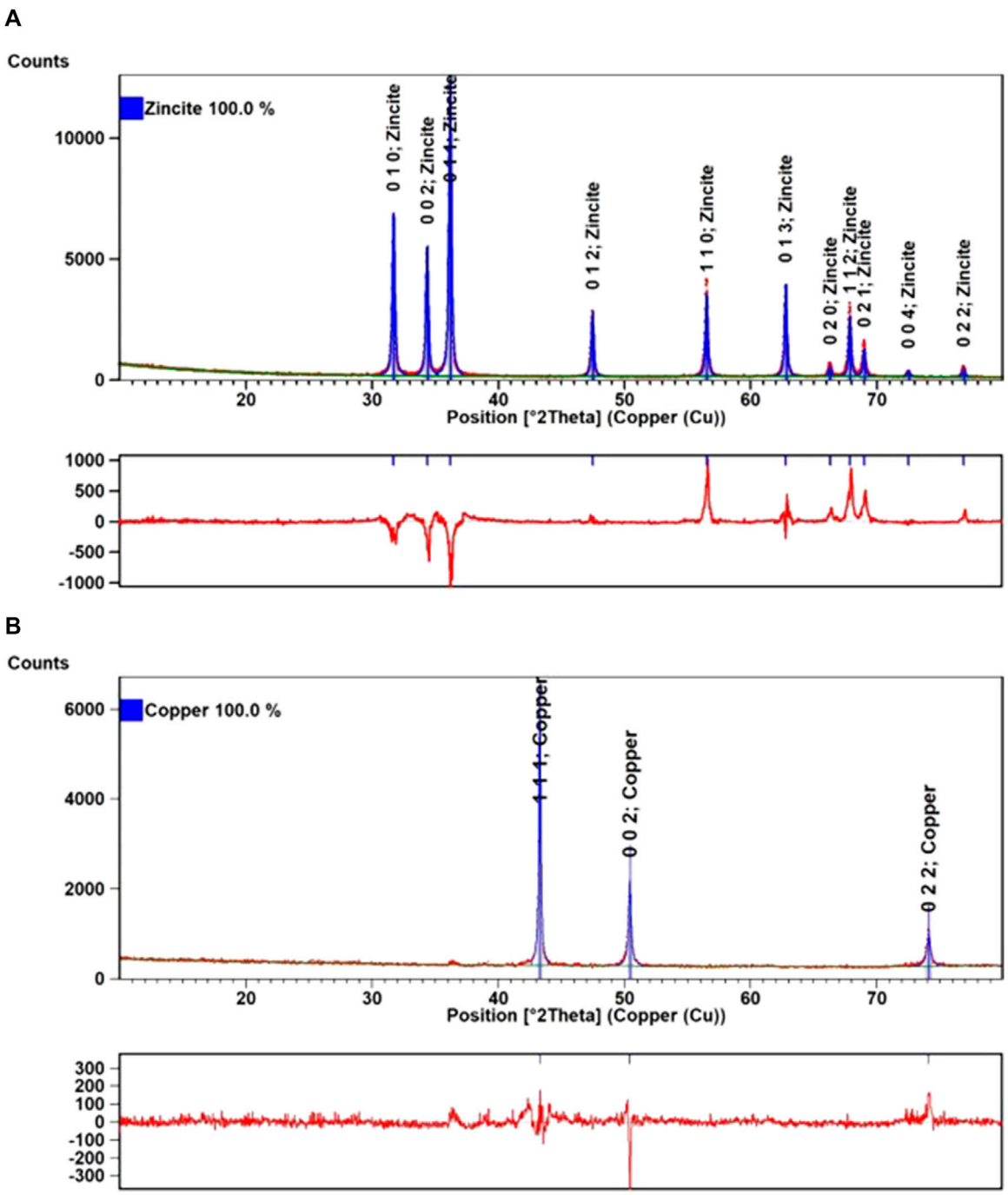

FIGURE 1
XRD diffractogram recorded on ZnO NPs **(A)** and Cu NPs **(B)**. Experimental data in red dots, refined data in blue lines, background in green lines, and the difference plot in red lines (below each diffractogram).

values 31.72° (100), 34.39° (002), 36.23° (101), and 47.44° (102) (Suresh et al., 2016; Oprea et al., 2011).

The XRD diffractogram (Figure 1B) recorded on Cu NPs showed an intense peak at 43.30, which has a (111) plane, and two low-intensity peaks at 50.42 and 74.03, characteristic of (200) crystallization planes (220). The peaks observed in the XRD diffractogram correspond to the findings in Suramwar (2012), demonstrating that the prepared Cu NPs are extremely pure, crystalline, and well-arranged in a specific orientation. No other peak due to impurities was observed.

The characteristics data provided by XRD, by using Rietveld refinement from HighScore Plus 3.0 software (Maqbool et al., 2022) and the COD database, are presented in Supplementary Table S1. In the case of copper powder, the formation of the pure cubic Cu (COD#: 96-900-8469) has been proved. This metallic powder has a crystallinity of 43.67% and a crystallite size of 34.18 ± 14.68 nm. In

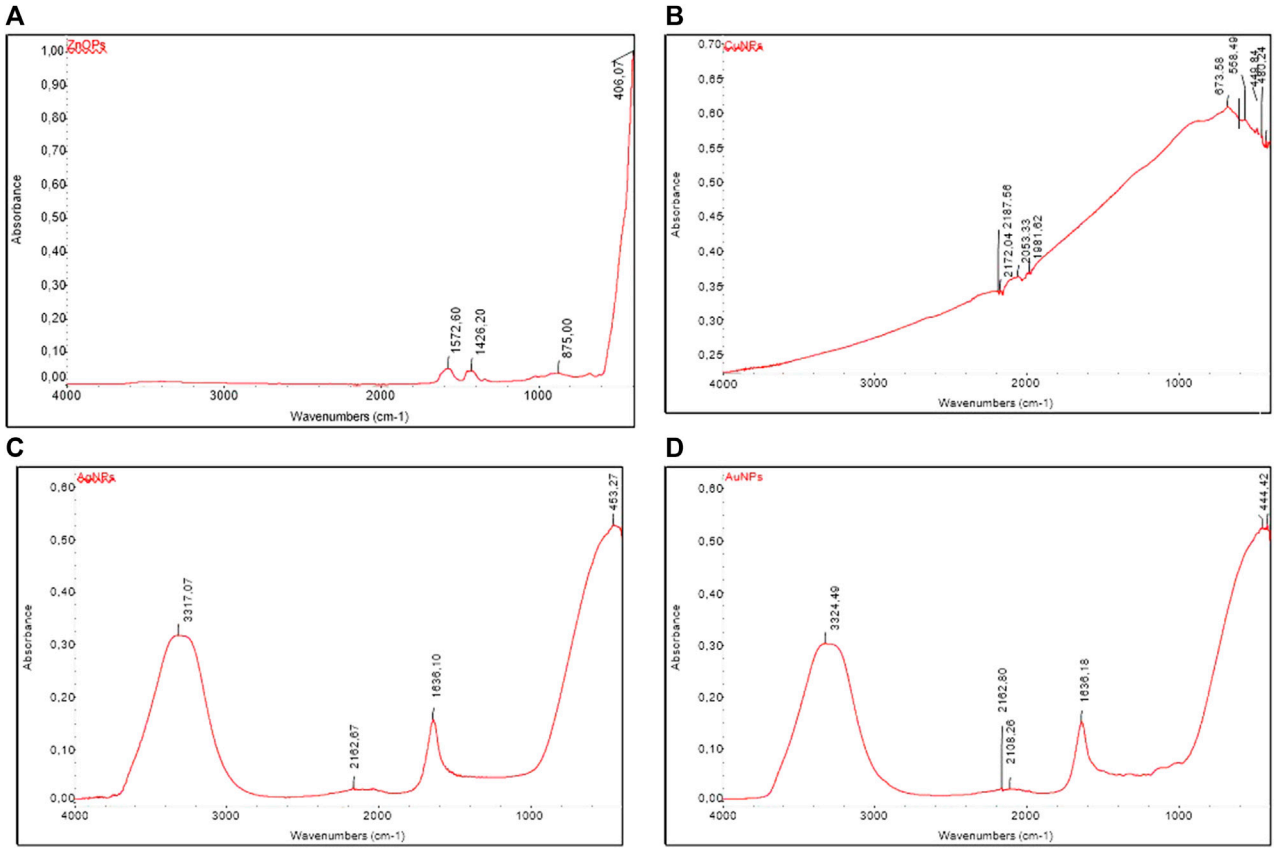

FIGURE 2
FTIR spectrum for ZnO NPs **(A)**, Cu NPs **(B)**, Au NPs **(C)**, and Ag NPs **(D)**.

the case of ZnO (COD#: 96-900-4182), hexagonal particles are obtained (P63/mc) having a crystallinity of 65.27% and a crystallite size of 35.88 ± 6.49 nm.

3.1.2 FTIR

In the FTIR spectrum (Figure 2A) of ZnO NPs, the characteristic bands of the stretching vibration of the Zn-O bond from approximately 415 to 480 cm^{-1} can be observed. The frequencies are consistent with the reported literature (Handore et al., 2014; Motelica et al., 2021) and correspond to the Zn-O characteristic stretching vibration. The weak peak from 677 cm^{-1} is due to Zn-OH bending vibration, while the peak from 875 cm^{-1} can be assigned to Zn^{2+} ions in tetrahedral symmetry. The weak peaks from 1,572 to 1,426 cm^{-1} are characteristic of the carboxylate group, asymmetric νas (COO) and symmetric νs (COO) vibrations. When the $\Delta\nu$ between the values of these two peaks falls in the interval 100–200 cm^{-1}, the carboxylate is in ionic form. This implies that some acetate ions remain adsorbed on the surface of NPs.

The spectrum recorded on Cu NPs (Figure 2B) is characterized by the presence of several absorption bands in the range 592–420 cm^{-1} caused by the νCu(II)-O stretching vibrations of copper oxide CuO. The absorption bands with maxima at 675 cm^{-1} can be attributed to νCu(I)-O vibrations, indicating the presence of some traces of Cu_2O oxide in the sample composition (Bharathi et al., 2020; Amali et al., 2022). As the XRD spectrum proves the purity of the sample, the presence of characteristic CuO and Cu_2O bands is due to the weak oxidation of Cu NPs upon contact with air, with their content probably up to 2%, and this is why even in FTIR the aforementioned peaks have low intensity. The absorption band with maxima in the range 2,190–2050 cm^{-1} is due to CO_2 absorption from the atmosphere. These results are consistent with the UV–Vis results.

The FTIR spectra recorded on the Au NPs synthesized using the hydrothermal method (Figure 2C) exhibit the characteristic bands being close to those reported by Khademi-Azandehi and Moghaddam (2015). The band at 1,636 cm^{-1} is characteristic of C=O and C=C stretching vibrations characteristic of the adsorbed organic compounds (citrate, lecithin, and ascorbate) (Stuart, 2004). The broad band centered at 3,416 cm^{-1} is characteristic of the O-H stretching vibration group (Alvarez-Ordónez and Prieto, 2012; Jabbar et al., 2020).

The FTIR spectra recorded on the Ag NPs synthesized using the Turkevich method (Figure 2D) exhibited characteristic bands centered at ~450, 1,636, and 3,320 cm^{-1}, these results being in good agreement with those reported by Jabbar et al. (2020). The band at 1,636 cm^{-1} is characteristic of C=O stretching vibrations () specific to the used PVP capping agent. The broad band from 3,420 cm^{-1} is characteristic of the associated hydroxyl stretching vibrations.

TABLE 1 DLS results obtained for Ag NPs.

Samples	Z (mv)	PD (index)	Diameter (nm)
Ag NPc (10 ppm)	−29.49	0.571	44.21
Ag NPt (100 ppm)	−19.60	0.250	44.23
Ag NPsol (1,000 ppm)	−35.45	0.571	32.83
Au NPs	−8.97	0.346	285,67
ZnO NPs	21.48	0.204	115.63
Cu NPs	−9.41	0.571	950.63

3.1.3 DLS

DLS is the most used method for determining the hydrodynamic diameter of particles suspended in solution. Particles with zeta potential between −10 and 10 mV are considered neutral and prone to aggregation, while particles with 10 mV ≤ |ζ|≤ 30 mV can repel each other and ensure incipient agglomeration; however, if |ζ| continues to increase, stability increases considerably, and aggregation is minimal or does not occur (Danaei et al., 2018). If we look at the zeta potential values (Table 1), they indicate that Au NPs are slightly electrically charged and prone to aggregation. The DLS method can be used to determine the degree of polydispersity of the particles. A polydispersity index (PI) of approximately 0.35 indicates moderate variations in particle sizes. In the case of Au NPs, the average diameter is approximately 285.76 nm, which probably means that these NPs are agglomerated (Table 1).

The values of the zeta potential indicate a reasonable-to-good stability of Ag NPs, the zeta potential being −19.60, −29.79, and −35.45 mV, which leads to a sufficiently high repulsion (Table 1), and the values of the PI 0.25 or 0.57 indicate that the particles are quite monodispersed for PI = 0.25 and highly dispersed in the case of PI = 0.57. Thus, Ag NP (c, t, and sol) samples present diameter values much smaller than 100 nm (Table 1). The diameters of the particles have almost similar sizes (Table 1), demonstrating that even when we use three different concentration, of over 2 magnitude (from 10 to 1,000 ppm), constant sizes of Ag NPs could be obtained with a quite narrow size distribution, with an average diameter of 32–44 nm.

The zeta potential values (Table 1) indicate that Au NPs have a low zeta potential (−8.97 mV), are slightly electrically charged, and thus are prone to aggregation. Moreover, during the synthesis, these NPs are also able to agglomerate, and this is why their hydrodynamic size is much larger than that of Ag NPs. The DLS method can be used to determine the degree of polydispersity of the particles. A polydispersity index (PI) of approximately 0.35 indicates moderate variations in particle size. In the case of Au NPs, the average diameter is approximately 285 nm, which probably means that these NPs are agglomerated (Supplementary Table S1).

In the case of Cu NPs, the values of the zeta potential indicate a reasonable stability, the zeta potential being −9.41 mV, which leads to a sufficiently high repulsion and a mean diameter of ~950 nm (in good agreement with the microscopy data), and the values of the PI 0.571 indicate that the particles are quite monodispersed.

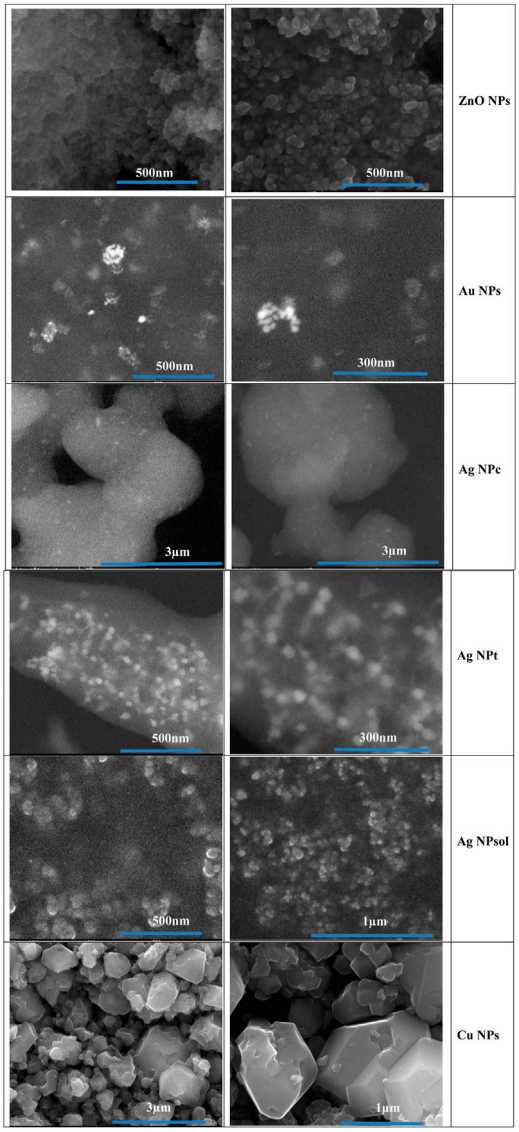

FIGURE 3
SEM images of metallic nanoparticles.

Considering the large size and the low zeta potential, it is obvious that these particles will be the least stable ones.

In the case of ZnO NPs, the average diameter is ~115 nm, and the value of the zeta potential is ~21 mV. The PI = 0.204 indicates that the particles are quite monodispersed. Based on these data, an incipient agglomeration of the ZnO NPs can be expected.

3.1.4 SEM

The recorded SEM images (Figure 3A) provided additional information on the size and morphology of the synthesized NPs. Based on these results, we can conclude that the obtained NPs are quite uniform, with a quite sharp size distribution and the size of the particles in the nano range (30–40 nm), comparable with the DLS data presented previously. The image shows ZnO NPs spherical in shape with a smooth surface.

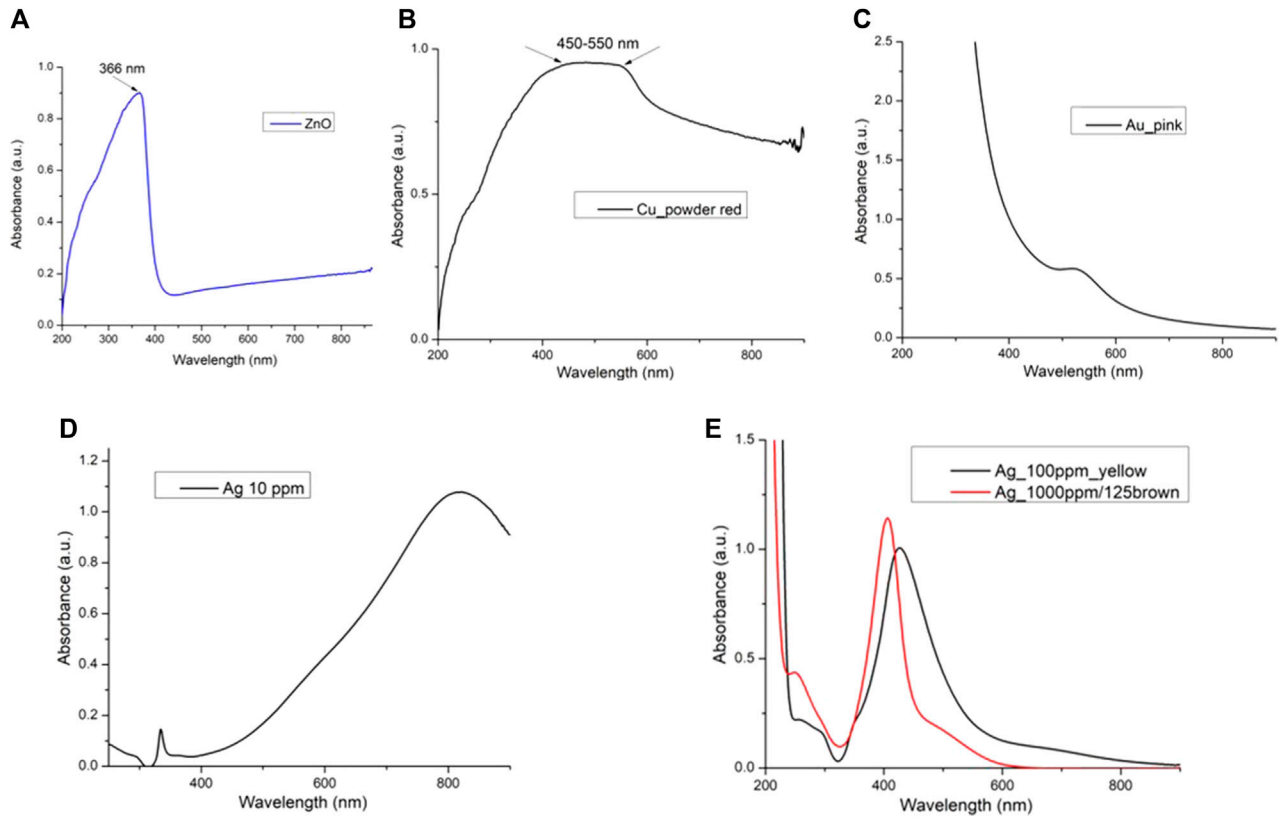

FIGURE 4
UV–Vis spectrum for ZnO NPs **(A)**, Cu NPs **(B)**, Au NPs **(C)**, and Ag NPs **(D, E)**.

The SEM images recorded on the Au NPs (Figure 3B) show the spherical shape and size of the NPs, which varies in the range of 9–25 nm. In addition, the SEM images confirm the agglomeration tendency of the Au NPs, being consistent with the DLS analysis.

In the SEM images (Figure 3C) recorded on Ag NPs, it can easily be observed that the size of NPs varies between 10 and 20 nm, and the results are consistent with the DLS data. Although the density of the NPs has significantly increased from the less concentrated colloidal solution (Ag NPc—10 ppm) to the most concentrated one (Ag NPsol—1,000 ppm), by corroborating these data with the DLS, it can be concluded that the particles remain independent, without concerning coalescence.

The SEM images recorded on the Cu NPs (Figure 3B) reveal the formation of the copper particles. These particles have polyhedral morphologies and are in the micrometric range, their size varying from 50 to ~1,000 nm (Figure 3D), and the results are in good agreement with the DLS data (Shantkriti, 2014).

3.1.5 UV–Vis

The shape of the spectrum (Figure 4A) is typical for white ZnO NPs. In the visible range, the absorbance of the sample is very low (white color), but below the range of 400 nm, the sample shows a strong absorbance, in the form of a single band, with the maximum value at 366 nm. To determine the width of the forbidden band, the Tauc method was applied, the experimental value being 3.227 eV, lower than the theoretical one of 3.37 eV, due to the existence of lattice defects. These lattice defects (most likely on the surface of the nanoparticles) generate and introduce additional energy levels inside the bandgap, ultimately leading to a decrease in its value. This is beneficial, as less energy is required to promote electrons from the bandgap valence in the conduction band and the generation of positive hole–electron pairs, responsible for the generation of reactive oxygen species (ROS). A higher level of ROS naturally leads to a high antimicrobial activity.

The UV–Vis spectrum for Cu NPs (Figure 4B) shows a broad absorption band, with the maximum located between 450 and 550 nm due to the surface plasmon resonance (SPR). The position is not clearly defined because the spectrum is recorded on powder and not as a colloidal solution. The surface plasmon resonance is influenced by the refractive index of the surrounding medium, in this case air; the stabilizing coating; and other Cu NPs, which leads to a broad band.

The UV–Vis spectra recorded on the pink Au NP colloidal solution present a single band in the UV–Vis spectrum (Figure 4C), NPs with spherical morphology and dimensions lower than 20 nm. The shape of the absorption band at 517 nm (generated by the SPR) indicates that the solution is stable and the NPs are not agglomerated, demonstrating a good stabilizing surface coating.

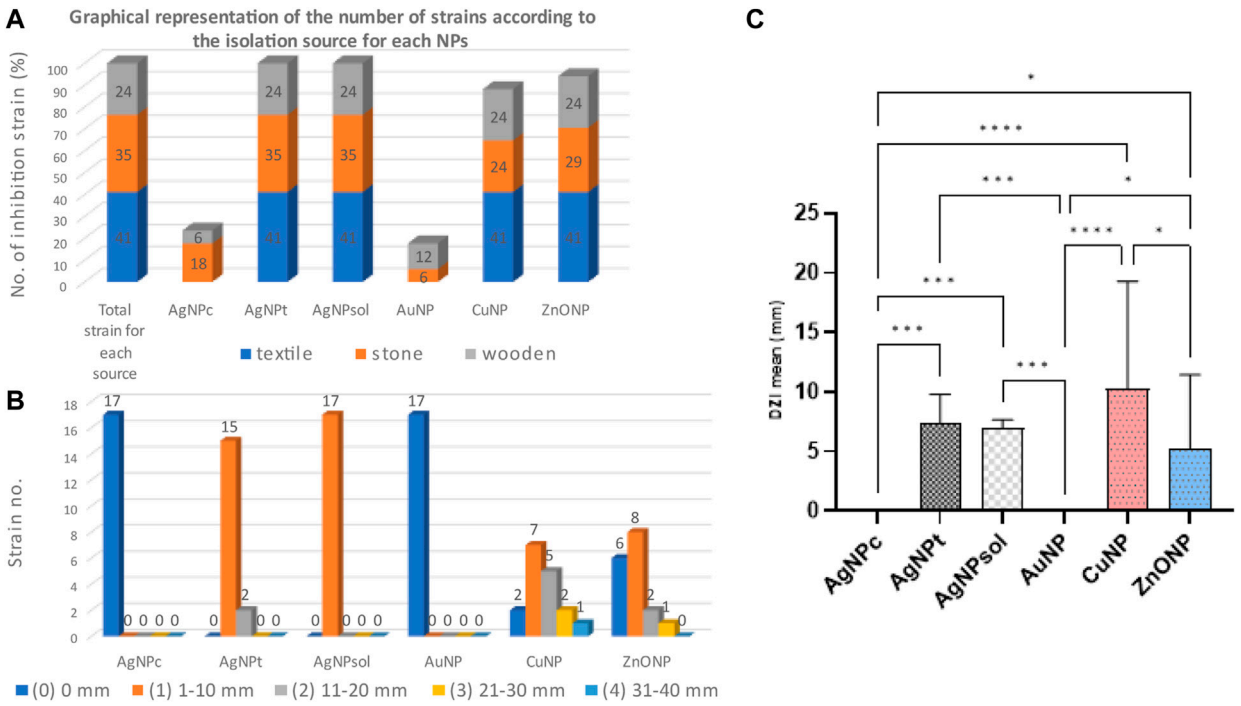

FIGURE 5
Inhibitory activity of NPs against bacterial strains expressed as a percentage of inhibited strains and related to the isolation source **(A)** and arbitrary units **(B)**. Statistical analysis between NPs **(C)** (where *$p < 0.05$, **$p < 0.01$, ***$p < 0.001$, and ****$p < 0.0001$).

TABLE 2 Of MIC values (μg/mL) of NP solutions against deteriogenic bacterial strains.

Strains	MIC (μg/mL)					
	Ag NPc	Ag NPt	Ag NPsol	Au NPs	Cu NPs	ZnO NPs
B. atrophaeus BB	50	0.78	19.5	17	312	39
B. megaterium S1R	12.5	0.39	0.9	114	156	78
B. megaterium MTR 20	25	0.39	0.9	114	234	78
B. megaterium MTR 12	6.25	0.19	0.9	228	156	78
B. pumilus B11	50	0.78	15.6	114	1,250	10,000
B. megaterium S23D	6.25	0.19	0.9	114	117	78
B. megaterium S3R	12.5	0.39	0.9	42.75	156	78
Bacillus spp. S6RA	12.5	0.39	0.9	7.1	312	78
B. pumilus OS7C	50	0.19	7.8	114	625	39
B. pumilus B3E	50	0.19	11.7	228	937.5	78
B. pumilus S2R	50	0.19	5.85	114	625	10,000
B. cereus C16156	50	0.39	0.9	14	1,250	10,000

The blue Ag NPc sample obtained by reduction with sodium borohydride has a UV–Vis spectrum (Figure 4D) with a broad absorption band, centered at 818 nm. The positioning of the SPR, at a wavelength higher than 800 nm, is specific to silver nanoparticles with triangular morphology (Condorelli et al., 2021). For the yellow Ag NPt sample, the UV–Vis spectrum (Figure 4E) indicates the position of the band corresponding to the SPR at 426 nm. The shape of the band is specific to spherical Ag NPs, with dimensions below 20 nm (Le et al., 2012). For the brown Ag NPsol, multiple dilution was necessary to allow measuring the absorbance, which was higher than the limit of the device. Figure 4E shows the spectra recorded after the 125-fold dilution and identified the band corresponding to

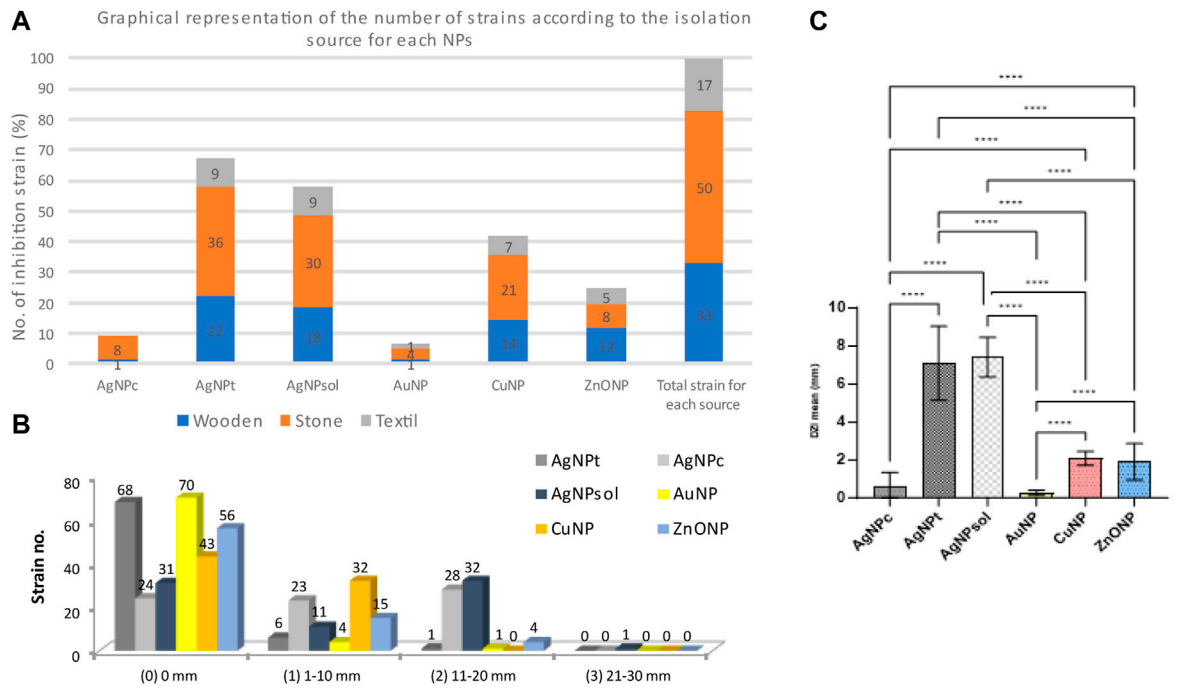

FIGURE 6
Inhibitory activity of NPs against microfungal strains expressed as a percentage of inhibited strains and related to the isolation source **(A)**, arbitrary units **(B)**, and statistical analysis between NPs **(C)** (where *$p < 0.05$, **$p < 0.01$, ***$p < 0.001$, and ****$p < 0.0001$).

the SPR at 406 nm, a value close to those reported in the literature for Ag NPs with spherical morphology and dimensions below 10 nm (Panda et al., 2018).

3.2 Antibacterial activity

The *qualitative* testing of NP solutions analyzed against a total number of 17 bacterial strains, isolated from stone (six), wood (four), and paper objects, textiles, wood, and ceramics from two museum collections (seven), evidenced a generally low and similar efficiency of the two types of Ag NPs, i.e., Ag NPt and Ag NPsol solutions ($p > 0.05$, Figure 5C), with the exception of one strain (*B. subtilis* MTR33U) being more susceptible to the Ag NPt solution (Supplementary Table S2, Figure 5B). The precentage of inhibited strains by NPs related to the isolation source could be found in Figure 5A. The mean of DIZs (diameters of inhibition zones) was significantly higher for Cu NPs than for Au NPs ($p < 0.0001$), Ag NPc ($p < 0.0001$), and ZnO NPs ($p < 0.05$).

3.2.1 Quantitative evaluation of the NP antibacterial activity against bacterial strains

Most of the bacterial strains tested were sensitive to Ag NPt and Ag NPsol solutions, with values of 0.19–0.78 (μg/mL) and 0.9–19.5 (μg/mL), respectively. The best antibacterial activity was observed for Ag NPt against *B. pumilus* strains. Ag NPc showed weaker activity than the rest of the Ag NPs (Table 2).

The Au NP solution showed antimicrobial activity at MIC values of 7.1–228 (μg/mL), being more active on the *Bacillus* spp. S6RA strain (isolated from textile material), and *B. cereus* encoded C16156 (isolated from a stone object). The ZnO NP solution inhibited the development of bacterial strains at concentrations of 39–10,000 (μg/mL), having a moderate activity against *B. atrophaeus* BB and *B. pumilus* OS7C strains (MIC = 39 μg/mL), both isolated from stone heritage objects and inactive against *B. pumilus* B11, *B. pumilus* S2R, and *B. cereus* C16156. The Cu NPs proved effective at MIC values of 1,250–117 μg/mL (Table 2), the strain of *B. megaterium* S23D (isolated from a textile material) being the most sensitive. Among the strains tested, the most resistant was the *B. pumilus* strain coded B11, isolated from a wooden museum object.

3.3 Antifungal activity

The qualitative screening of the antifungal activity of Ag NPc, Ag NPt, and Ag NPsol, Au NPs, Cu NPs, and ZnO NPs was determined on a total number of 75 microfungal strains isolated from different heritage objects: stone (38), wood (25), and museum collections (13) (Supplementary Figure S1).

The efficiency of the NP solutions was in descending order: Ag NPt = Ag NPsol > Cu NP > ZnO NP > Ag NPc > Au NP (Figure 6A). The Ag NPt and Ag NPsol solutions showed the highest efficiency (arbitrary unit identification 3) (Figure 6B). The efficiency of the NP solutions on the microfungal strains tested related to the isolation source demonstrated that Ag NPt and Ag NPsol showed high activity regardless of the origin of the strain, inhibiting more than 50% of the tested strains. The efficiency of ZnO NPs and Cu NPs was higher on strains recovered from wooden heritage objects, followed by those isolated from museum objects. In the case

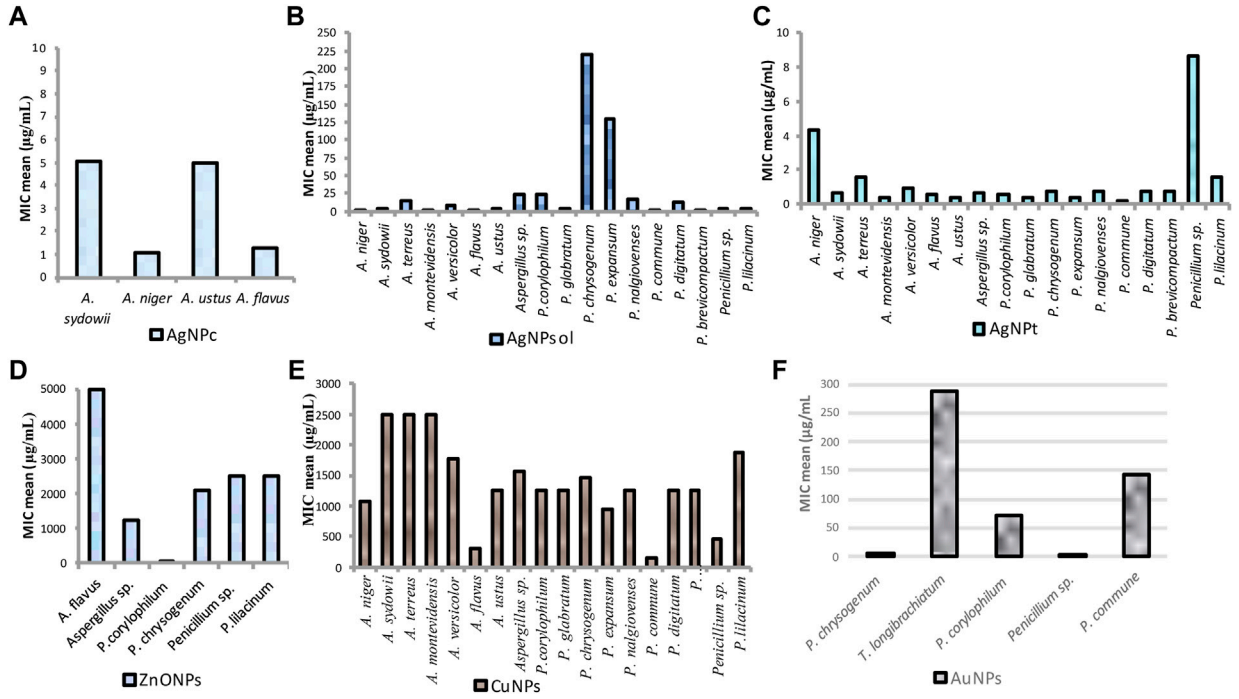

FIGURE 7
Graphical representation of the MIC values of the Ag NPc **(A)**, Ag NPsol **(B)**, Ag NPt **(C)**, ZnO NPs **(D)**, Cu NPs **(E)**, and Au NPs **(F)** against different microfungi strains.

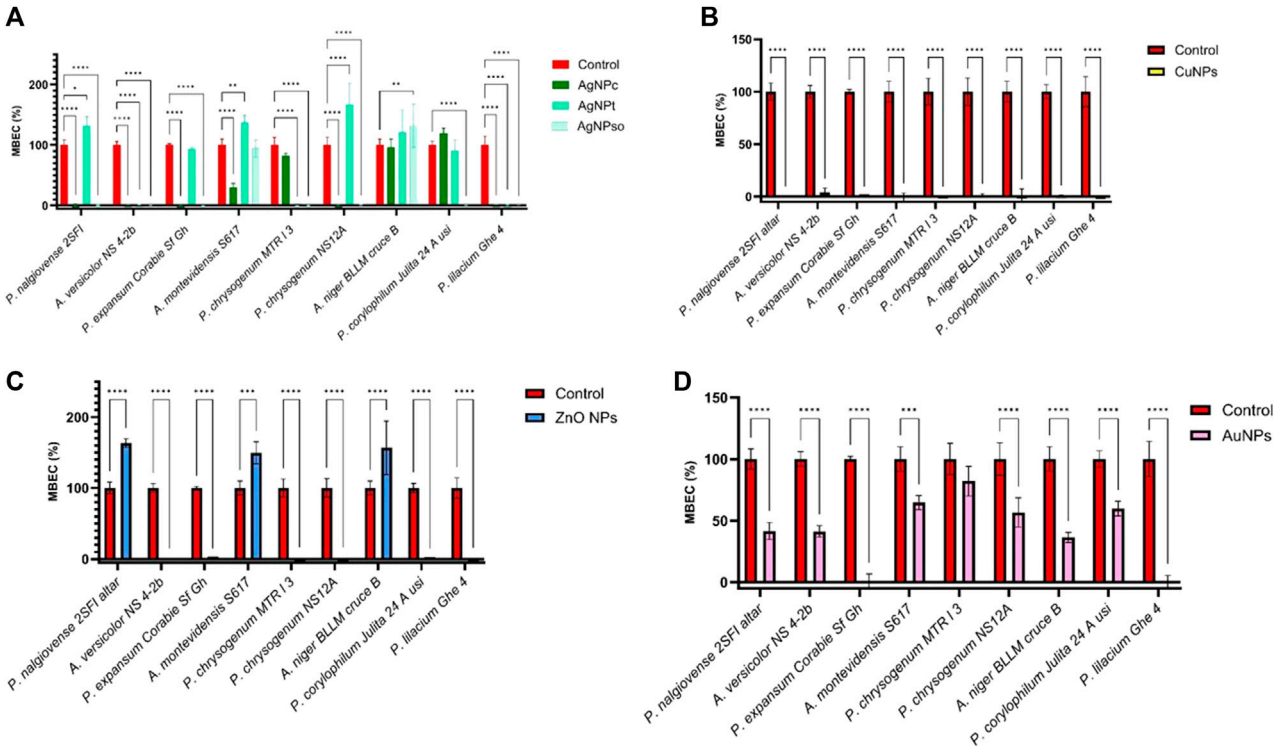

FIGURE 8
Graphical representation of the inhibitory effect on the adhesion capacity of filamentous fungi strains treated with MIC/2 of Ag NP **(A)**, Cu NP **(B)**, ZnO NP **(C)**, and Au NP **(D)** solutions.

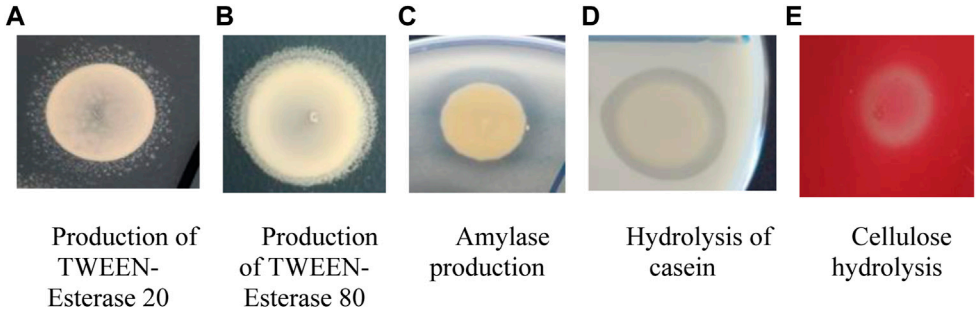

FIGURE 9
Aspect of positive relations for the analyzed enzymes specific to strains of *Bacillus* spp.

of Ag NPc and Au NPs, respectively, the efficiency was limited regardless of the origin of the strains. The strains sensitive to Ag NPt were isolated mainly from the stone heritage objects (Figure 6A). The mean of DIZs (diameters of inhibition zones) was significantly higher for Ag NPt and Ag NPsol than for Au NPs ($p < 0.0001$), Ag NPc ($p < 0.0001$), Cu NPs ($p < 0.0001$), and ZnO NPs ($p < 0.0001$) (Figure 6C).

Quantitative evaluation of the antifungal activity of the NPs against deteriogenic strains isolated from wooden and stone buildings and museum collection objects demonstrated that seven strains of *Aspergillus* showed sensitivity to Ag NPc action (mean MIC value = 1.05–5.3 µg/mL) (Figure 7A). Ag NPts demonstrated their effectiveness against strains of *Penicillium* (n = 32; mean MIC value = 0.19–8.59 µg/mL), *Aspergillus* (n = 17; mean MIC value = 0.39–4.36 µg/mL), and *P. lilacinum* (mean MIC value < 5 µg/mL) (Figure 8C). The Ag NPsols were active against *Aspergillus* strains (average MIC values = 0.97–23.76 µg/mL) and *P. commune* (MIC value < 1 µg/mL) and inactive on *P. chrysogenum* strains (mean MIC value >200 µg/mL). In the case of *Purpureocillium* spp., the average MIC value was below 5 µg/mL (Figure 8B).

The Au NPs inhibited the mycelial development of a limited number of microfungal strains belonging to the *Penicillium* genus (Figure 7F). The Cu NPs were effective on 42.66% of the strains belonging to the *Penicillium* (18), *Aspergillus* (13), and *Purpureocillium* (1) genera, the most sensitive being *A. flavus* strains (312.5 µg/mL) (Figure 7E). The ZnO NPs demonstrated their effectiveness against *P. corylophilum* strains (MIC = 32.55 µg/mL) (Figure 7D). In Figures 7B, C were highlighted the MIC mean for AgNPsol and AgNPt.

3.4 Influence on the microbial adherence to the inert substratum

The Ag NPc were active against 60% of the strains at a concentration of 6.25 µg/mL, Ag NPt at 0.78 µg/mL–0.19 µg/mL against 40%, Ag NPsol at 3.9–0.9 µg/mL, while the Au NPs inhibited the adhesion capacity of 50% of the tested strains, at 0.85 – 0.425 µg/mL, much lower than the MIC values. Cu NPs and ZnO NPs were active at concentrations similar to the MIC values, except for two strains of *B. pumilus*, for which ZnO was active at 9.75 µg/mL.

In order to highlight the impact of NPs on the adhesion capacity of filamentous fungi strains to the inert substrate, a total number of 17 strains isolated from stone and wooden churches or museum heritage objects were selected. Among these, it was highlighted that the strains encoding *P. corylophilum* Julita 2B, *P. corylophilum* BLLM12, *Aspergillus* spp. NS11c, *P. digitatum* OS16, *P. brevicompactum* CP2, *P. corylophilum* Julita 29, *P. lilacinum* Ghe 6a, and *P. corylophilum* BLLM 32 did not show adhesion capacity to the inert substrate.

In the case of Ag NPs, it can be observed that Ag NPsol showed the highest efficiency, followed by Ag NPc. In contrast, Ag NPt solutions showed a lower effect, in some cases even promoting microbial adhesion (in the case of *P. chrysogenum* MTR l3, *A. montevidensis* S617, and *P. nalgiovense* 2SFI strains). The best inhibitory effect was observed in *P. lilacinum* Ghe 4 and *A. versicolor* NS4-2B strains for all three Ag NP solutions (Figure 8A).

The Cu NPs significantly reduced the adhesion capacity of the tested microfungal strains to the inert substrate, with the percentage of MBEC values being below 10% (Figure 8B).

The ZnO NP solutions reduced the adhesion capacity to the inert substrate of the microfungal strains, except for *P. nalgiovense* 2SFi, *A. montevidensis* S617, and *A. niger* BLLM cross B strains, in which the percentage of MBEC was significantly higher compared to the control (Figure 8C). Similarly, the Au NP solution showed an inhibitory effect, the best results being obtained in the case of *P. expansum* Corabie Sf. Ghe and *P. lilacinum* Ghe 4 strains, respectively (Figure 8D).

3.5 The effect of NPs on microbial strain metabolic activity

The evaluation of the influence of Au NPs, Ag NPs, Cu NPs, and ZnO NPs on the production of enzymes and acids was carried out on specific culture media monitored during 6 days to record the occurrence of a positive reaction.

3.5.1 Bacterial strains

The detection of esterases was investigated on Tween 20 and Tween 80 supplemented media, the positive reaction being evidenced by the appearance of insoluble Ca^{2+} oleate crystals formed by the released fatty acids with the Ca^{2+} ions (Figure 9A).

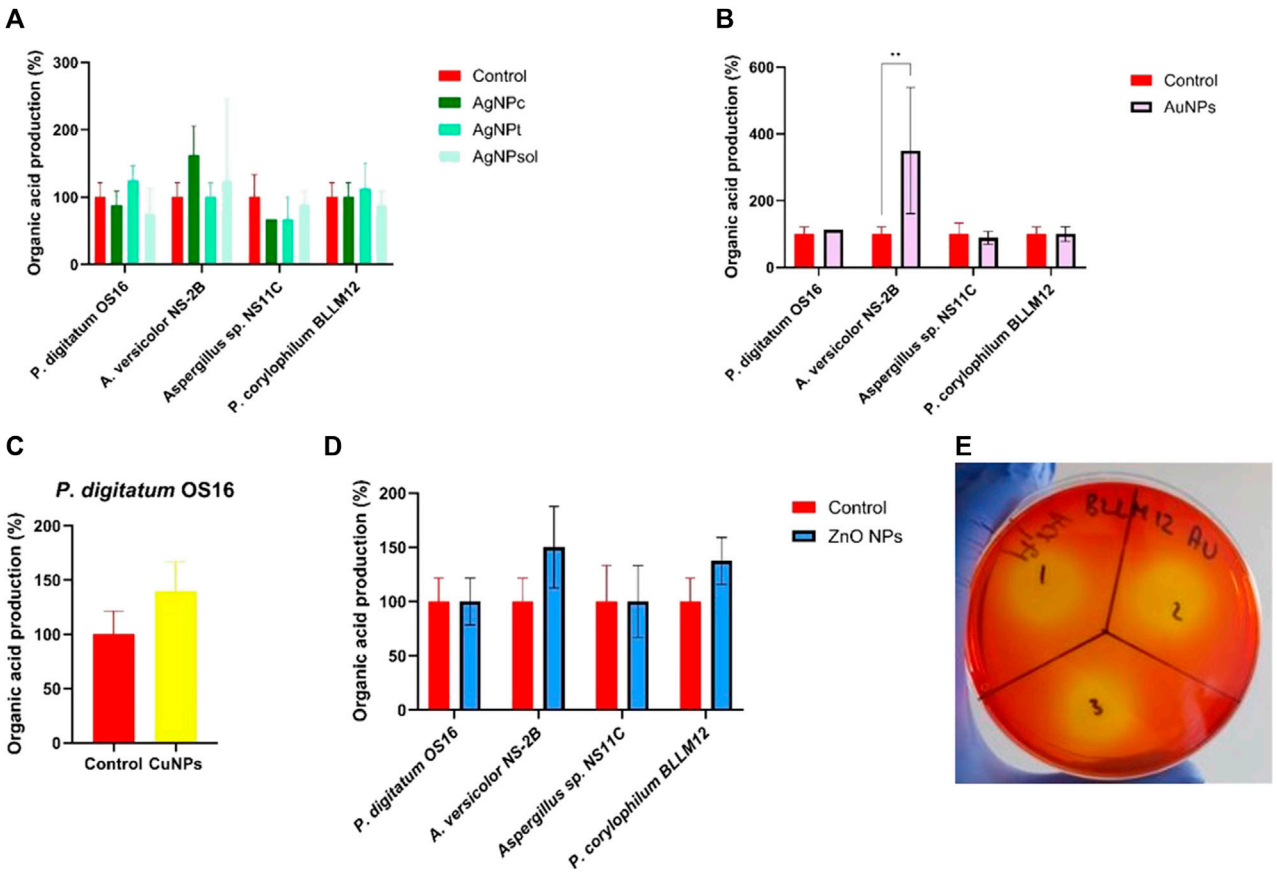

FIGURE 10
Graphic representation of the inhibitory effect of Ag NP **(A)**, Au NP **(B)**, Cu NP **(C)**, and ZnO NP **(D)** solutions and plate aspect **(E)** on the ability of filamentous fungi strains to secrete organic acids.

The cultivation in the presence of subinhibitory concentrations of Au and Cu NP solutions stimulated the production of Tween 80 esterase in the case of the *B. pumilus* S2R strain and inhibited it in the case of the *B. pumilus* B11 strain. The amylase was evidenced on starch-supplemented media, the positive reaction being highlighted by the appearance of a halo around the culture spot (Figure 9C), which has been inhibited by the Cu NPs and Au NPs in the case of *B. megaterium* S3R and *B. cereus* C16156 strains. The caseinase and cellulase expression has not been influenced by the analyzed NPs (Figure 9E). In Figure 9B is the aspect of positive reaction for production of esterase, using Tween-80. The aspect of casein production is highlighted in Figure 9D.

3.5.2 Microfungal strains

Regarding the production of organic acids, it was highlighted that the inhibitory action of Ag NPs varies depending on the analyzed species. Thus, the best results were obtained for one *Aspergillus* strain encoded NS11C in which the three types of Ag NPs reduced its ability to secrete extracellular organic acids. In the case of the other strains, the inhibitory effect was low (Figure 10A). The cultivation of microfungal strains in the presence of Cu NPs even at subinhibitory concentrations affected their ability to grow on the specific agar medium for acid production. In the case of the *P. digitatum* OS16 strain, exposure to subinhibitory concentrations of Cu NPs stimulated the production of organic acids into the culture medium (Figure 10C).

Exposure of the strains to subinhibitory concentrations of Au NPs did not influence their ability to secrete organic acids, except for the *A. versicolor* NS4-2B strain, in which the effect was stimulatory (Figure 10B). Similarly, in the case of ZnO NPs, the inhibitory effect was not highlighted (Figure 10D). The plate aspect on the ability of filamentous fungi strains to secrete organic acid is presented in Figure 10E.

The Ag NPs stimulated the proteolytic activity exhibited by the two *Aspergillus* strains, the strongest stimulatory effect being induced by Ag NPsol (Figure 11A). In the case of *Penicillium* strains, although the values are higher compared to the control, the differences are not statistically significant, and therefore, it can be considered that they do not have a significant influence. The Cu NPs did not significantly influence the ability to hydrolyze casein, except for the *P. expansum* A5-52 strain, in which they induced a strong inhibitory effect (Figure 11B). In addition, Au NPs (Figure 11C) and ZnO NPs (Figure 11D) did not influence the ability of the strains to hydrolyze casein, except for *P. expansum* A5-52 and *A. versicolor* NS4-2B strains, respectively, in which the

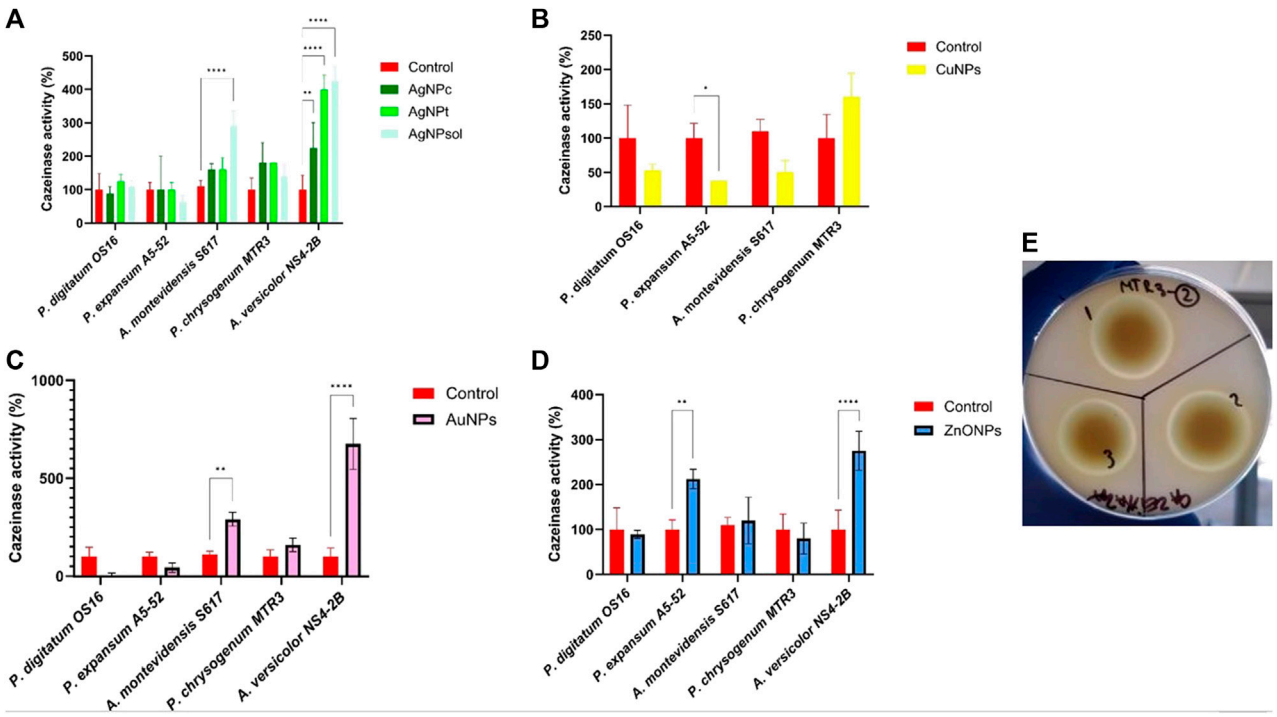

FIGURE 11
Graphic representation of the inhibitory effect of Ag NPs **(A)**, Cu NPs **(B)**, Au NPs **(C)**, and ZnO NPs **(D)** and plate aspect **(E)** on the ability of filamentous fungi strains to hydrolyze casein.

stimulation of caseinase production was observed. The plate aspect on the ability of filamentous fungi strains to hydrolyze casein is presented in Figure 11E.

Regarding amylase, in the case of the *P. expansum* A5-52 strain, exposure to subinhibitory concentrations of Ag NPsol, Au NP, and ZnO NP solutions stimulated the strain's ability to hydrolyze the α-1,4-glycosidic bonds in the starch structure (Figures 12A, C, D). From the Figure 12B, it can be seen that CuNPs intensify amylase activity in the case of *P. chrysogenum* MTR3 strain. The plate aspect on the ability of filamentous fungi strains to hydrolyze starch is highlighted in Figure 12E.

3.6 Ecotoxicity

The ZnO NPs (10 mg/mL) and the control did not influence the *Allium cepa var rubra* bulbs growth; a non-statistically significant stimulation of the growth was observed in the case of Cu NPs (10 mg/mL) and Ag NPt (0.1 mg/mL), respectively, and a reduction of the growth was revealed in the case of Ag NPsol (1 mg/mL) (Table 3). An increase in weight gain was observed for all variants. Non-significant differences between the pre-test and post-test period for the same type of NPs were observed.

4 Discussion

Most of the organic and inorganic artifacts are susceptible to different phenomena such as discoloration caused by climatic factors, surface powdering, cracking, reduced strength, increased porosity, microbial colonization, and degradation (Fistos et al., 2022). Microbial communities grown on organic and inorganic artifacts increase substrate deterioration through physico-chemical processes and cause destructive effects on the integrity of the monument itself and the objects inside; at the same time, they also pose a danger to the health of visitors and those attending the religious services (Marcu et al., 2021). Previous data have shown the strong potential of Ag, Au, Cu, ZnO NPs, and TiO_2 to develop next-generation strategies for wood and stone artifact preservation (Nair et al., 2013; Moya et al., 2014; Borges et al., 2018; Khadiran et al., 2022; Nair et al., 2022; Alfieri and Canosa, 2023; Pietka et al., 2022), due to their bactericidal and antibiofilm effects, high stability, and low volatility, ensuring long-term usage and good biocompatibility (Arreche et al., 2017; Becerra et al., 2018; Aldosari et al., 2019; Schifano et al., 2020). According to a recent study, the most recurrently applied NMs for the preservation and treatment of the deteriorated cultural heritage object substrates (stone, glass, wood, paper, and textiles) are in the decreasing order of the frequency TiO_2 NPs, Ag NPs, ZnO NPs, SiO_2 NPs, Cu NPs, MgO NPs, zinc-derivatives, carbon NMs, and layered double hydroxides (Franco-Castillo et al., 2021).

In the present study, we aimed to assess the capacity of Ag, Au, Cu, and ZnO NPs to inhibit microbial growth, biofilm development, and metabolic activity (cellulase, protease, esterase, phenoloxidase, and organic acid production) for their potential application in the preservation of the cultural heritage objects in Romania. For validating their potential, we have used a significant collection of

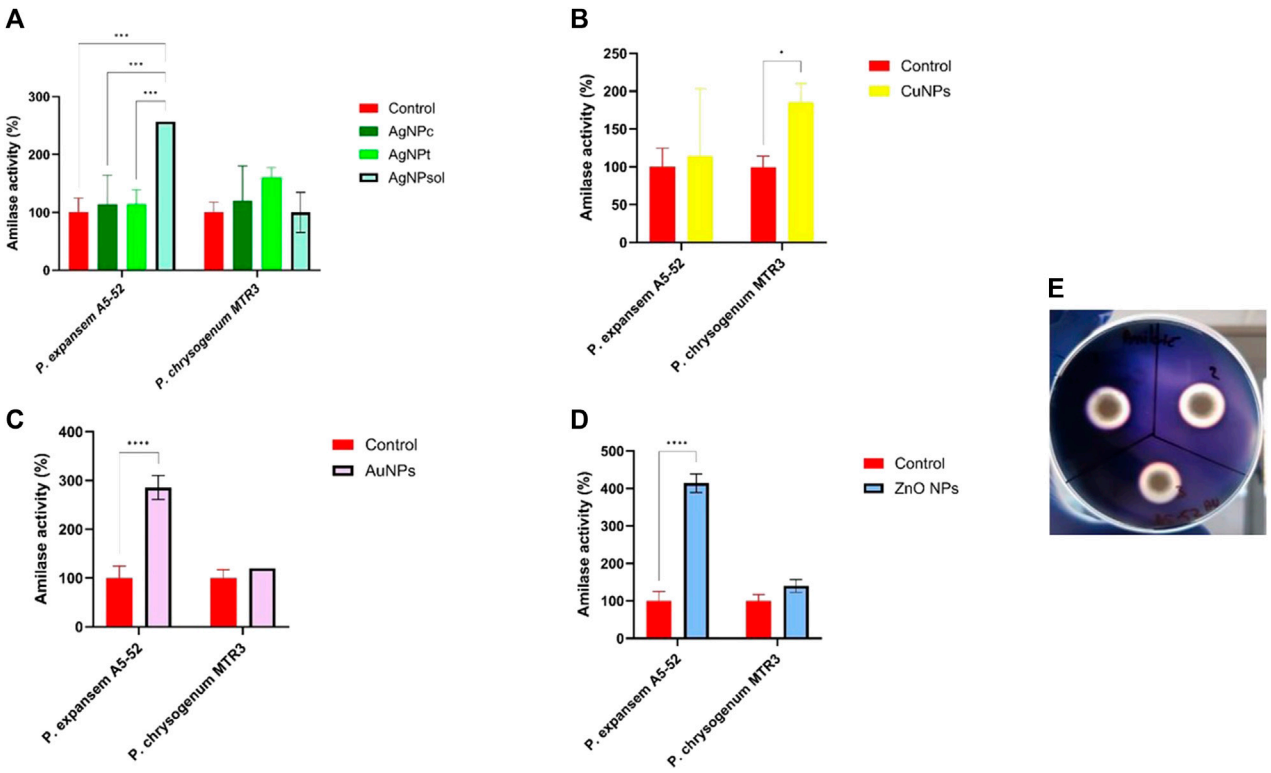

FIGURE 12
Graphic representation of the inhibitory effect of Ag NP **(A)**, Cu NP **(B)**, Au NP **(C)**, and ZnO NP **(D)** solutions and plate aspect on the ability of filamentous fungi strains to hydrolyze starch.

TABLE 3 Daily average weight gain of the bulbs for the pre-test and post-test periods.

Sample set	The pre-test period		The post-test period		*t*-test
	The daily average weight gain g)	Coeff. var	The daily average weight gain g)	Coeff. var	
ZnO NPs (10 mg/mL)	79.18 ± 44.21	55.82735	74.20 ± 24.71	71.86331	0.832116
Cu NPs (10 mg/mL)	59.15 ± 30.81	52.09532	73.58 ± 40.54	71.86331	0.540465
Au NPs (0.2 mg/mL)	33.67 ± 26.19	77.79864	43.46 ± 15.48	71.86331	0.677283
Ag NPt (0.1 mg/mL)	31.85 ± 27.22	85.46244	44.09 ± 23.10	71.86331	0.603211
Ag NPsol (1 mg/mL)	45.88 ± 30.73	66.97352	30.37 ± 8.18	26.93692	0.510847
Blank sample set (in distilled water)	45.71 ± 32.85	71.86331	47.07 ± 16.47	34.99022	0.953814

microbial strains isolated from historical Romanian wooden and stone churches dating back to the 17th century, which were in a poor state of conservation. Most of the investigated churches face the problem of heating and do not have a ventilation and air conditioning system; therefore, the indoor microclimate is mostly conditioned by the external weather conditions, which can lead to the chemical and biological deterioration with a potential risk on the health of parishioners. The NPs have been first obtained by classical, solvothermal, and Turkevich wet chemical synthesis methods and characterized by X-ray diffraction (XRD), infrared spectroscopy (FTIR), dynamic light scattering (DLS), scanning electron microscopy (SEM), and UV–Vis spectroscopy. ZnO NPs were obtained by precipitation, while Au and Ag NPs were obtained by reduction in the presence of proper stabilization agents. In fact, in the case of Au NPs, the size in DLS is much larger than that determined in SEM, which means that the agglomeration is high, a result also supported by zeta potential. In the case of Ag NPs, for all the three used concentrations, from 10 to 1,000 ppm, the diameter was in the nanometric range and had a good stability, predicted by the zeta potential being below ~ −20 mV.

The increasing concentration of precursors was directly proportional to the NP size, similar to other studies. For

instance, Usman et al., starting from a precursor solution of 0.05 M, obtained particles of 2–350 nm (also depending on the concentration of the capping agent), while, in this study, at a precursor concentration of 0.4 M, the size increased up to ~1,000 nm. It is important to mention that considering the final application, a higher concentration can assure longer protection and thus require only one application to treat the monument's surface. There are several physical, chemical, and hybrid processes that may be used for developing various kinds of NPs. Although the use of harmful chemicals severely restricts the biomedical uses of NPs, particularly in the clinical domains, physical and chemical approaches are still more common in their manufacturability. Therefore, it is crucial to create trustworthy, non-toxic, and environmentally acceptable technologies for synthesizing NPs in order to facilitate their biological uses (Li et al., 2011). Several green synthesis techniques of NPs have been reported using bacterial strains, various plants, or derived reducing agents (Sidorowicz et al., 2023). For instance, Sastry et al. described the extracellular manufacture of Au NPs by the actinomycete *Thermomonospora* spp. and the filamentous fungi *F. oxysporum*, respectively (Mukherjee et al., 2002; Ahmad et al., 2003). When using fungi, such as *Verticillium*, *Fusarium oxysporum*, or *Aspergillus flavus*, Ag NPs have been produced as a film, in solution, or collected on the surface of the cell (Li et al., 2011). Additionally, microalgae are currently being used as a source of metabolites that can contribute to the ecologically friendly and less expensive production of a variety of NPs. Due to their abundance of secondary metabolites that act as capping and reducing agents, microalgae make great candidates for the synthesis of a range of NPs (Sidorowicz et al., 2022). Over the classical wet synthesis technique, these methods present some advantages such as, for instance, eliminating the use of synthetic chemicals. Unfortunately, a major drawback is related to the lower productivity of green synthesis methods. In addition to difficulties to be adapted for large-scale production, the NP solutions obtained by green methods could contain compounds that may induce degradation, coloring of the surface, or promote the adhesion of other unwanted products (Sidorowicz et al., 2022; Ying et al., 2022).

The antimicrobial efficiency of the obtained NP solutions was tested against 17 bacterial and 75 fungal strains isolated from stone and wood heritage buildings and museum collection objects. The bacterial adhesion to the inert substratum is the initial stage of biofilm formation. Within these microbial communities' complex interactions between microorganisms, communicating with each other and reacting to environmental conditions take place. One of the most important consequences of the biofilm's formation is the increased resistance of bacteria not only to environmental factors but also to the action of antimicrobial substances. Therefore, this study also analyzed the ability of tested NPs to inhibit the adhesion capacity of *Bacillus* spp. strains to an inert substrate.

The results of the antibacterial activity against the 17 *Bacillus* spp. strains demonstrated that the highest efficiency was observed for Ag NPt against *B. pumilus* strains; most of the tested bacterial strains were sensitive to Ag NPt and Ag NPsol. The Ag NPc, Au NPs, and ZnO NPs showed weaker activity than the rest of the Ag NPs. Concerning the antimicrobial activity of the proposed NP solutions against the filamentous fungi belonging to the *Aspergillus*, *Penicillium*, *Purpureocillium*, and *Trichoderma* genera, the decreasing order by efficiency of the tested NP solutions was as follows: Ag NPt = Ag NPsol > Cu NP > ZnO NP > Ag NPc > Au NP. The Ag NPt and Ag NPsol showed high efficiency regardless of substrate type, inhibiting more than 50% of the strains. The strains sensitive to Ag NPt were isolated mainly from the stone heritage buildings. The efficiency of ZnO NPs and Cu NPs was higher on strains recovered from wooden buildings than those from museum objects. Depending on the tested strain species and their isolation sources, a different inhibition level was observed. For example, in *P. chrysogenum* strains, known as very resistant to oxidative stress through the secretion of a high amount of catalase and glutathione peroxidase (Emri et al., 1997), a higher resistance level to all investigated NPs was identified (Supplementary Figure S1).

The mechanism of antibacterial activity of Ag NPs is well-documented, having particular relevance in the biomedical field, due to their antibacterial, antifungal, antiviral, anti-inflammatory, anticancer, antiangiogenic, and antioxidant properties. However, besides the biomedical applications of Ag NPs, they have shown an inhibitory effect against filamentous fungi belonging to *Aspergillus, Rhizopus, Penicillium, Cladosporium, Alternaria,* and *Mucor* genera; yeasts, such as *Rhodotorula* and *Candida;* and bacterial strains belonging to the *Bacillus* genus recovered from the surface of archival documents and historical objects and from air microbiota and surfaces in different museums and archives from Warsaw and Lodz, Poland (Gutarowska et al., 2012). Bellissima et al. (2014) investigated the ability of Ag NPs and of a silane derivative to reduce the growth and *B. subtilis* viability on the surface of stone artworks and demonstrated a 50%–80% reduction in cell viability. It was noticed that Ag NPs mixed with two types of consolidation polymers revealed antifungal activity against *A. niger* and thus represent a potent consolidation agent of the historic monuments and artifacts (Essa and Khallaf, 2014). The efficiency of disinfection with Ag NPs of historical textile materials from sisal, cotton, and wool (Plata Museum, Argentina) demonstrated a reduction of microbial load depending on the microorganism group and the degree of colonization, the most resistant being different *Bacillus* species and conversely, the most susceptible were filamentous fungi from *Penicillium* and *Cladosporium* spp. (Pietrzak et al., 2016). A total growth inhibition of *A. versicolor* and C. *cladosporioides* on biodeteriorated bricks and a high efficiency regarding the biofilm removal were demonstrated using Ag NPs coated with two silane precursors (Gámez-Espinosa et al., 2020). Regarding their mechanism of action, it has been shown that the Ag NPs accumulate on the cell wall and membrane, causing cytoplasm shrinking and membrane disruption. The Ag NPs can also bind to membrane proteins and affect membrane permeability, the respiration chain, and ion transport (Tang and Zheng, 2018). In certain situations, Ag NPs can enter the cell, where they can interact with DNA and/or with intracellular proteins, thus interfering with transcription, translation, and sugar metabolism (Rinna et al., 2015). In the case of Gram-positive bacteria, such as those included in this study, it could be expected that their thicker cell wall with a high content of peptidoglycan decreases the efficiency of Ag NPs (Rai et al., 2012), but our study has shown the contrary. Regarding the mechanism of antimicrobial action against filamentous fungi, available studies are limited, but it has been proven that exposure to Ag NPs causes prominent injury associated with membrane disruption of mycelia, as well as with ROS generation,

downregulation of stress enzymes, and disruption of endogenic antioxidant machinery (Pereira et al., 2014; Kumari et al., 2019).

ZnO NPs revealed antifungal (against *A. niger, A. versicolor, Rhizopus nigricans, Saccharomycetes*, and *Mucor* spp.) and antibacterial (on both Gram-positive and Gram-negative bacteria) activity in different studies (Evans et al., 2008; David et al., 2020) and provided paper protection against UV radiation, fungi, and bacteria (Ditaranto et al., 2015; Afsharpour and Imani, 2017). The complete inhibition of *A. niger* growth by the ZnO nanocomposite (ZnO NPs and Estel 1000, Estel 100, Silo 111-based consolidating agent/water repellent material) by *in vitro* assays was demonstrated, while the *in situ* assay on stone did not provide significant results, the nanocomposite based on ZnO and nanocellulose composite was used as the coating solution of a newspaper from 1960, inducing an increased color stability and antimicrobial efficiency filamentous fungi strains (Jia et al., 2019). The efficiency of biosynthesized Ag and ZnO NPs on the microbial growth of a total of 26 microbial strains isolated and identified by molecular methods from a deteriorated archaeological manuscript in Cairo, Egypt, as well as on preventing the cellulase production in *B. subtilis* and *P. chrysogenum* strains, and the color and structural changes of the substrate was demonstrated, sustaining that the proposed solution could be included as a constituent of paper manufacturing for future manuscripts (Roveri et al., 2018; Fouda et al., 2019). Roveri et al., in 2018 investigated the efficiency of a hydrophobized silica with AgO and ZnO NPs on treated stone substrates from three lithotypes (Apuan marble, Balegem limestone, and Schlaitdorf sandstone), emblematic of different European geological and environmental areas and have revealed a high efficiency of the proposed solution in the reduction of *B. cereus* microbial load (in the case of Balegem and Schlaitdorf specimens) and a lower efficiency in the case of Apuan marble. The antimicrobial activity of ZnO NPs is highly dependent on size, crystalline structure, and concentration (Xie et al., 2011; Lallo da Silva et al., 2019), and the direct contact of these NPs with the cell walls causes disruption of cell integrity (Adams et al., 2006; Zhang et al., 2007) and release of Zn^{2+} ions, ROS formation, and disruption of mitochondrial function (Kasemets et al., 2009; Li et al., 2011). For fungi, the internalization of ZnO NPs occurs through direct diffusion and endocytosis. After internalization, the Zn^{2+} release can penetrate the nuclear membrane, causing chromosome damage and cell death (Lallo da Silva et al., 2019). For *P. expansum*, the exposure to ZnO NPs is associated with conidiophores and conidia-forming inhibition (He et al., 2011). Similar results were obtained for other *Penicillium* spp., such as *P. digitatum* (Supplementary Figure S1). Tayel et al. (2011) showed that Gram-positive bacteria are more susceptible to ZnO NPs, while the presence of lipopolysaccharides in the outer membrane of Gram-negative bacteria can counteract the inhibitory effect of ZnO NPs.

The efficiency of Cu NPs and Cu NPs coated with commercial consolidants and water-repellents (Silo 111, Acrilico 30, and Estel 1000) was evaluated on different archaeological stone types (sandstone, marble, and plaster) in Florence, Italy, demonstrating their ability of reducing the recolonization, but their inefficiency in the prevention of fungal growth and of the biofilm formation (Pinna et al., 2018). In the case of Cu NPs, the mechanism is similar to the one described for ZnO NPs, the inhibition effects being associated with the Cu^{2+} release, interaction with the peptidoglycan through electrostatic attraction, disruption of cell membrane, and DNA damage (Rispoli et al., 2010; Bogdanović et al., 2014). For *B. subtilis,* a high sensitivity to Cu NPs was demonstrated, possibly due to the greater abundance of functional groups (amines and carboxyl groups) with an affinity to react with the copper ions and NPs (Ruparelia et al., 2008). Our study has also demonstrated a high sensitivity of *B. pumilus, B. subtilis,* and *B. megaterium* strains to these NPs. The antifungal activity of Cu NPs is accompanied by mycelium color changes due to the melanin or carotenoid production as a response to oxidative stress (Meghana et al., 2015; Lopez-Lima et al., 2021).

Au NPs have shown antibacterial ability against both Gram-positive and Gram-negative bacteria by degrading the membrane potential as a result of ATPase inhibition and by inhibiting the binding of tRNA to ribosomes (Slavin et al., 2017; Nisar et al., 2019; Gu et al., 2021). The Au NPs possibly interact with phosphorus-containing bases in the DNA or sulfur-containing proteins in the membrane, causing the interruption in DNA repairing mechanisms, replication, and, ultimately, cell death (Tan et al., 2011). Ahmad et al. (2013) have shown that Au NPs exhibit size-dependent antifungal activity and greater biocidal action against fungal isolates, the best results being obtained for Au NPs of 7 nm in size. The size of Au NPs included in our study is higher (9–25 nm), and this might be the reason for the absence of inhibition in the case of fungi and only limited activity against bacterial strains.

The investigated bacteria and filamentous fungi strains included in the study presented various effects on the production of metabolites responsible for the biodeterioration process. Thus, for each enzyme type, several representative microbial strains were selected to determine whether Ag, Au, Cu, and ZnO NPs influence their ability to produce and secrete the enzyme or the organic acids in the culture medium. According to the obtained results, the treatment of microbial cultures with subinhibitory concentrations of NPs leads either to inhibition or stimulation, the results being different depending on the investigated strain, the tested metabolite, or the substrate.

To be applied to heritage objects, the proposed NP solutions should also be investigated for their ecotoxicity. The *Allium* test demonstrated that the obtained NPs are eco-friendly. Although the purpose of the present study was different, the ecotoxicity test results show that those NPs that did not negatively affect *A. cepa var rubra* bulb growth have the potential to be used as nano-fertilizers (NFs), which appears promising. The use of nanoparticles to improve plant growth, nutrient absorption, and agricultural yield is referred to as NFs according to recent studies. The drawbacks of conventional chemical fertilizers can be solved using a nanohybrid construction like NFs. The NFs transfer nutrients to the plants in an intelligent way, demonstrating their superiority over bulky chemical fertilizers in terms of agricultural output and environmental sustainability. Depending on the methods of administration and the characteristics of the particles, plants can absorb NFs through their roots or leaves (Babu et al., 2022). When applied to the foliage of rice, ZnO NPs have shown ideal success in overcoming zinc shortage. Additionally, ZnO boosted dehydrogenase enzyme activity and enhanced growth and yield characteristics. NPs are efficient in supplying crops with micronutrients (Paramo et al., 2020). Numerous NFs, including Cu, K, Zn, and Fe, have demonstrated remarkable targeted delivery when used at a particular concentration for various kinds of crops (Nongbet et al., 2022).

Most of the previous Romanian works investigated the microbial communities colonizing different Romanian heritage objects from wood, stone, or from the museum and library collections or evaluated the degradation level of different objects but not the alternative preservation treatment solutions based on NPs (Budrugeac et al., 2007; Budrugeac et al., 2014; Budrugeac et al., 2017; Lupan et al., 2014; Georgescu et al., 2016; Gomoiu et al., 2016; Gomoiu et al., 2016; Ilies et al., 2018a; Ilies et al., 2018b; IIies et al., 2021; Indrie et al., 2019; Onet et al., 2020; Neamtu et al., 2021).

In this context, to the best of our knowledge, this is the first study to demonstrate the efficiency of alternative solutions based on Ag, Au, Cu, and ZnO NPs against biodeteriogenic microbial strains recently isolated from a significant number of Romanian wood and stone cultural heritage churches, with a representative geographical coverage, dating from different periods, as well as from two museum collections. The obtained results proved the potential of the tested NPs, especially of Ag NPs (the nanoparticles with the lowest size), to develop efficient and economical alternative solutions for heritage restoration treatments, showing high antimicrobial efficiency against the prevalent etiological agents of Romanian heritage objects. Although preliminary, these results are yet essential for the development of optimized strategies to combat deteriogenic microorganisms and for the preservation of cultural heritage objects. Further research will involve exploring the effectiveness of these NPs on museum-like surfaces from which the microorganisms were recovered, as well as the dynamics of microbial biofilm formation on the respective surfaces.

Data availability statement

The original contributions presented in the study are included in the article/Supplementary Material; further inquiries can be directed to the corresponding author.

Author contributions

VC: data curation, investigation, writing–original draft, conceptualization, formal analysis, and methodology. AD: data curation, formal analysis, investigation, and writing–original draft. LM: data curation, formal analysis, investigation, writing–original draft, and methodology. LuM: data curation, formal analysis, investigation. CC: data curation, formal analysis, investigation, and writing–original draft. AS: data curation, formal analysis, investigation, writing–original draft, and methodology. IG-B: formal analysis, investigation, methodology, writing–original draft, conceptualization, funding acquisition, resources, supervision, and validation. IP: formal analysis, investigation, writing–original draft, data curation, and visualization. IB: data curation, formal analysis, investigation. MP: data curation, formal analysis, investigation, writing–original draft, methodology, and validation. IM: data curation, investigation, writing–original draft, software, and visualization. NI: data curation, investigation, visualization, writing–original draft, and supervision. DG-C: formal analysis, investigation, and writing–original draft. LD: funding acquisition, supervision, validation, visualization, writing–review and editing, and conceptualization. DF: funding acquisition, project administration, resources, supervision, validation, visualization, and writing–review and editing. OO: formal analysis, investigation, methodology, data curation, software, and writing–original draft. AF: supervision, visualization, writing–review and editing, formal analysis, investigation, methodology, resources, and validation. TE: conceptualization, supervision, visualization, and writing–review and editing. MC: conceptualization, funding acquisition, resources, supervision, validation, visualization, and writing–review and editing.

Funding

The authors declare that no financial support was received for the research, authorship, and/or publication of this article.

Acknowledgments

The authors acknowledge the financial support of the Research Projects PN-III-P2-2.1-PED-2021-2526 (736 PED/2022), PN-III-P2-2.1-PED-2021-0627 (591PED/2022), and C1.2. PFE-CDI.2021-587 (41PFE/30.12.2021).

Conflict of interest

The authors declare that the research was conducted in the absence of any commercial or financial relationships that could be construed as a potential conflict of interest.

Publisher's note

Supplementary material

The Supplementary Material for this article can be found online at: https://www.frontiersin.org/articles/10.3389/fmats.2023.1272869/full#supplementary-material

References

Abdel-Daim, M. M., Eissa, I. A. M., Abdeen, A., Abdel-Latif, H. M. R., Ismail, M., Dawood, M. A. O., et al. (2019). Lycopene and resveratrol ameliorate zinc oxide nanoparticles-induced oxidative stress in Nile tilapia, *Oreochromis niloticus*. *Environ. Toxicol. Pharmacol.* 69, 44–50. doi:10.1016/j.etap.2019.03.016

Adams, L. K., Lyon, D. Y., and Alvarez, P. J. J. (2006). Comparative eco-toxicity of nanoscale TiO2, SiO2, and ZnO water suspensions. *Water Res.* 40, 3527–3532. doi:10.1016/j.watres.2006.08.004

Afsharpour, M., and Imani, S. (2017). Preventive protection of paper works by using nanocomposite coating of zinc oxide. *J. Cult. Herit.* 25, 142–148. doi:10.1016/j.culher.2016.12.007

Ahmad, A., Senapati, S., Khan, M. I., Kumar, R., and Sastry, M. (2003). Extracellular biosynthesis of monodisperse gold nanoparticles by a novel extremophilic actinomycete, Thermomonospora sp. *Langmuir* 19, 3550–3553. doi:10.1021/la026772l

Ahmad, T., Wani, I. A., Lone, I. H., Ganguly, A., Manzoor, N., Ahmad, A., et al. (2013). Antifungal activity of gold nanoparticles prepared by solvothermal method. *Mater. Res. Bull.* 48, 12–20. doi:10.1016/j.materresbull.2012.09.069

Aldosari, M. A., Darwish, S. S., Adam, M. A., Elmarzugi, N. A., and Ahmed, S. M. (2019). Using ZnO nanoparticles in fungal inhibition and self-protection of exposed marble columns in historic sites. *Archaeol. Anthropol. Sci.* 11, 3407–3422. doi:10.1007/s12520-018-0762-z

Alfieri, P. V., and Canosa, G. (2023). Nano-sustainable protective system to control biological colonization for wood heritage. Preprints 2023, 2023061071. Available at: https://doi.org/10.20944/preprints202306.1071.v1.

Alvarez-Ordónez, A., and Prieto, M. (2012). *Fourier transform infrared spectroscopy in food microbiology*. New York, NY: Springer. doi:10.1007/978-1-4614-3813-7

Amali, R. K. A., Lim, H. N., Ibrahim, I., Zainal, Z., and Ahmad, S. a. A. (2022). A copper-based metal-organic framework decorated with electrodeposited Fe2O3 nanoparticles for electrochemical nitrite sensing. *Mikrochim. Acta* 189, 356. doi:10.1007/s00604-022-05450-y

Arreche, R., Bellotti, N., Deyá, C., and Vázquez, P. (2017). Assessment of waterborne coatings formulated with sol-gel/Ag related to fungal growth resistance. *Prog. Org. Coatings* 108, 36–43. doi:10.1016/j.porgcoat.2017.04.007

Aziz, F., Ihsan, A., Nazir, A., Ahmad, I., Bajwa, S. Z., Rehman, A., et al. (2017). Novel route synthesis of porous and solid gold nanoparticles for investigating their comparative performance as contrast agent in computed tomography scan and effect on liver and kidney function. *IJN* 12, 1555–1563. doi:10.2147/IJN.S127996

Babu, S., Singh, R., Yadav, D., Rathore, S. S., Raj, R., Avasthe, R., et al. (2022). Nanofertilizers for agricultural and environmental sustainability. *Chemosphere* 292, 133451. doi:10.1016/j.chemosphere.2021.133451

Balakumaran, M. D., Ramachandran, R., Jagadeeswari, S., and Kalaichelvan, P. T. (2016). *In vitro* biological properties and characterization of nanosilver coated cotton fabrics–An application for antimicrobial textile finishing. *Int. Biodeterior. Biodegrad.* 107, 48–55. doi:10.1016/j.ibiod.2015.11.011

Barberio, M., Veltri, S., Imbrogno, A., Stranges, F., Bonanno, A., and Antici, P. (2015). TiO2 and SiO2 nanoparticles film for cultural heritage: conservation and consolidation of ceramic artifacts. *Surf. Coatings Technol.* 271, 174–180. doi:10.1016/j.surfcoat.2014.12.045

Becerra, J., Zaderenko, A. P., Sayagués, M. J., Ortiz, R., and Ortiz, P. (2018). Synergy achieved in silver-TiO2 nanocomposites for the inhibition of biofouling on limestone. *Build. Environ.* 141, 80–90. doi:10.1016/j.buildenv.2018.05.020

Bella, M., Randazzo, D., Carlo, E., Barresi, G., and Palla, F. (2015). Monitoring biological damage on paper-based documents in the historical archive of the palermo astronomical observatory. *Conservation Sci. Cult. Herit.* 15, 85–94. doi:10.6092/issn.1973-9494/7121

Bellissima, F., Bonini, M., Giorgi, R., Baglioni, P., Barresi, G., Mastromei, G., et al. (2014). Antibacterial activity of silver nanoparticles grafted on stone surface. *Environ. Sci. Pollut. Res.* 21, 13278–13286. doi:10.1007/s11356-013-2215-7

Bharathi, E., Sivakumari, G., Kamalakkannan, J., Karthikeyan, B., and Senthilvelan, S. (2020). Synergetic execute pressure, temperature on mixed Ac/Ag@CuO and its multi properties of solar light elucidation and antibacterial activity by hydrothermal technique. *Mater. Sci. Energy Technol.* 3, 407–419. doi:10.1016/j.mset.2020.02.002

Blee, A., and Matisons, J. (2008). Nanoparticles and the conservation of cultural heritage. *Mater. Forum* 32, 121–128.

Bogdan, A., Chambre, D., Copolovici, D. M., Bungau, T., Bungau, C. C., and Copolovici, L. (2022). Heritage building preservation in the process of sustainable urban development: the case of brasov medieval city, Romania. *Sustainability* 14, 6959. doi:10.3390/su14126959

Bogdanović, U., Lazić, V., Vodnik, V., Budimir, M., Marković, Z., and Dimitrijević, S. (2014). Copper nanoparticles with high antimicrobial activity. *Mater. Lett.* 128, 75–78. doi:10.1016/j.matlet.2014.04.106

Borges, C. C., Tonoli, G. H. D., Cruz, T. M., Duarte, P. J., and Junqueira, T. A. (2018). Nanoparticles-based wood preservatives: the next generation of wood protection? *CERNE* 24, 397–407. doi:10.1590/01047760201824042531

Budrugeac, P., Carşote, C., and Miu, L. (2017). Application of thermal analysis methods for damage assessment of leather in an old military coat belonging to the history museum of braşov—Romania. *J. Therm. Anal. Calorim.* 127, 765–772. doi:10.1007/s10973-016-5343-8

Budrugeac, P., Cucos, A., and Miu, L. (2014). Use of thermal analysis methods to asses the damage in the book bindings of some religious books from XVIII century, stored in Romanian libraries. *J. Therm. Anal. Calorim.* 116, 141–149. doi:10.1007/s10973-013-3414-7

Budrugeac, P., Miu, L., and Soukova, M. (2007). The damage in the patrimonial books from Romanian libraries. Thermal analysis methods and scanning electron microscopy. *J. Therm. Anal. Calorim.* 88, 693–698. doi:10.1007/s10973-006-8085-1

Carpino, C., Loukou, E., Andersen, B., Settino, J., and Arcuri, N. (2023). "Biodeterioration in historic buildings. Indoor environmental conditions and risk of fungal growth," in *Proceedings of the 2022 IMEKO TC4 international conference on metrology for Archaeology and cultural heritage* (Consenza, ITALY: IMEKO), 62–67. doi:10.21014/tc4-ARC-2022.013

Castillo, I. F., Guillén, E. G., de la Fuente, J. M., Silva, F., and Mitchell, S. G. (2019). Preventing fungal growth on heritage paper with antifungal and cellulase inhibiting magnesium oxide nanoparticles. *J. Mater. Chem. B* 7 (41), 6412–6419. doi:10.1039/c9tb00992b

Cennamo, P., Barone Lumaga, M. R., Ciniglia, C., Soppelsa, O., and Moretti, A. (2018). Heterotrophic components of biofilms on wood artefacts. *J. Wood Sci.* 64 (4), 417–426. doi:10.1007/s10086-018-1705-0

Condorelli, M., Scardaci, V., Pulvirenti, M., D'Urso, L., Neri, F., Compagnini, G., et al. (2021). Surface plasmon resonance dependent third-order optical nonlinearities of silver nanoplates. *Photonics* 8, 299. doi:10.3390/photonics8080299

Corbu, V. M., Gheorghe, I., Marinaş, I. C., Geană, E. I., Moza, M. I., Csutak, O., et al. (2021). Demonstration of Allium sativum extract inhibitory effect on biodeteriogenic microbial strain growth, biofilm development, and enzymatic and organic acid production. *Mol. (Basel, Switz.* 26, 7195. doi:10.3390/MOLECULES26237195

Corbu, V. M., Gheorghe-Barbu, I., Marinas, I. C., Avramescu, S. M., Pecete, I., Geană, E. I., et al. (2022). Eco-friendly solution based on rosmarinus officinalis hydro-alcoholic extract to prevent biodeterioration of cultural heritage objects and buildings. *Int. J. Mol. Sci.* 23, 11463. doi:10.3390/ijms231911463

Danaei, M., Dehghankhold, M., Ataei, S., Davarani, F. H., Javanmard, R., Dokhani, A., et al. (2018). Impact of particle size and polydispersity index on the clinical applications of lipidic nanocarrier systems. *Pharmaceutics* 10, 57. doi:10.3390/pharmaceutics10020057

Datcu, A. D., Ciobanu, D. G., Boros, B. V., Ostafe, V., and Ianovici, N. (2020). A new approach for phytotoxicity testing using Allium cepa bulbs. *Rom. Biotechnol. Lett.* 25, 1488–1494. doi:10.25083/rbl/25.2/1488.1494

David, M. E., Ion, R. M., Grigorescu, R. M., Iancu, L., and Andrei, E. R. (2020). Nanomaterials used in conservation and restoration of cultural heritage: an up-to-date overview. *Materials* 13 (9), 2064. doi:10.3390/ma13092064

Ditaranto, N., Werf, I. D., Picca, R. A., Sportelli, M. C., Giannossa, L. C., Bonerba, E., et al. (2015). Characterization and behaviour of ZnO-based nanocomposites designed for the control of biodeterioration of patrimonial stoneworks. *New J. Chem.* 39, 6836–6843. doi:10.1039/c5nj00527b

Emri, T., Pócsi, I., and Szentirmai, A. (1997). Glutathione metabolism and protection against oxidative stress caused by peroxides in Penicillium chrysogenum. *Free Radic. Biol. Med.* 23, 809–814. doi:10.1016/s0891-5849(97)00065-8

Essa, A. M. M., and Khallaf, M. K. (2014). Biological nanosilver particles for the protection of archaeological stones against microbial colonization. *Int. Biodeterior. Biodegr.* 94, 31–37. doi:10.1016/j.ibiod.2014.06.015

Evans, P., Matsunaga, H., and Kiguchi, M. (2008). Large-scale application of nanotechnology for wood protection. *Nat. Nanotechnol.* 3 (10), 577. doi:10.1038/nnano.2008.286

Fierascu, I., Mariana, R., Radu, M., Dima, S. O., Bunghez, I. R., Avramescu, S. M., et al. (2014). Comparative study of antifungal effect of natural extracts and essential oils of *Ocimum basilicum* on selected artefacts. *Rev. Roum. Chim.* 59, 207–211.

Fistos, T., Fierascu, I., and Fierascu, R. C. (2022). Recent developments in the application of inorganic nanomaterials and nanosystems for the protection of cultural heritage organic artifacts. *Nanomaterials* 12, 207. doi:10.3390/nano12020207

Fouda, A., Abdel-Maksoud, G., Abdel-Rahman, M. A., Salem, S. S., Hassan, S. E. D., and El-Sadany, M. A. H. (2019). Eco-friendly approach utilizing green synthesized nanoparticles for paper conservation against microbes involved in biodeterioration of archaeological manuscript. *Int. Biodeterior. Biodegrad.* 142, 160–169. doi:10.1016/J.IBIOD.2019.05.012

Franco-Castillo, I., Hierro, L., de la Fuente, J. M., Seral-Ascaso, A., and Mitchell, S. G. (2021). Perspectives for antimicrobial nanomaterials in cultural heritage conservation. *Chem* 7, 629–669. doi:10.1016/j.chempr.2021.01.006

Gambino, M., Ahmed, M. A. A. A., Villa, F., and Cappitelli, F. (2017). Zinc oxide nanoparticles hinder fungal biofilm development in an ancient Egyptian tomb. *Int. Biodeterior. Biodegrad.* 122, 92–99. doi:10.1016/j.ibiod.2017.05.011

Gámez-Espinosa, E., Barberia-Roque, L., Obidi, O. F., Deyá, C., and Bellotti, N. (2020). Antifungal applications for nano-additives synthesized with a bio-based approach. *Adv. Nat. Sci. Nanosci. Nanotechnol.* 11, 015019. doi:10.1088/2043-6254/ab790f

Georgescu, M., Gheorghe, I., Curutiu, C., Lazar, V., Bleotu, C., and Chifiriuc, M. C. (2016). Virulence and resistance features of *Pseudomonas aeruginosa* strains isolated from chronic leg ulcers. *BMC Infect. Dis.* 16, 92. doi:10.1186/s12879-016-1396-3

Gheorghe, I., Avram, I., Maria Corbu, V., Măruțescu, L., Popa, M., Balotescu, I., et al. (2021). *In vitro* evaluation of MgB2 powders as novel tools to fight fungal biodeterioration of heritage buildings and objects. *Front. Mater.* 7, 458. doi:10.3389/fmats.2020.601059

Gheorghe, I., Sârbu, I., Pecete, I., Blăjan, I., and Balotescu, I. (2020). Multi-level characterization of microbial consortia involved in the biodeterioration of wooden and stone Romanian heritage churches. *Conservation Sci. Cult. Herit.* 20, 289–308. doi:10.6092/ISSN.1973-9494/12805

Gomoiu, I., Enache, I., Cojoc, R., Mohanu, I., and Mohanu, D. (2016). "Biodeterioration of wooden churches from Romania. Case studies: the church from amărăști, vâlcea county," in *Microbes in the spotlight: Recent progress in the understanding of beneficial and harmful microorganisms*. Editor A. Mendez-Vilas (Boca Raton, FL, USA: Brown Walker Press), 51–55.

Gu, X., Xu, Z., Gu, L., Xu, H., Han, F., Chen, B., et al. (2021). Preparation and antibacterial properties of gold nanoparticles: a review. *Environ. Chem. Lett.* 19, 167–187. doi:10.1007/s10311-020-01071-0

Gutarowska, B., Skora, J., Zduniak, K., and Rembisz, D. (2012). Analysis of the sensitivity of microorganisms contaminating museums and archives to silver nanoparticles. *Int. Biodeterior. Biodegrad.* 68, 7–17. doi:10.1016/j.ibiod.2011.12.002

Handore, K., Bhavsar, S., Horne, A., Chhattise, P., Mohite, K., Ambekar, J., et al. (2014). Novel green route of synthesis of ZnO nanoparticles by using natural biodegradable polymer and its application as a catalyst for oxidation of aldehydes. *J. Macromol. Sci. Part A* 51, 941–947. doi:10.1080/10601325.2014.967078

He, L., Liu, Y., Mustapha, A., and Lin, M. (2011). Antifungal activity of zinc oxide nanoparticles against Botrytis cinerea and Penicillium expansum. *Microbiol. Res.* 166, 207–215. doi:10.1016/j.micres.2010.03.003

Ilies, D. C., Oneț, A., Marcu, F. M., Gaceu, O. R., Timar, A., Baias, S., et al. (2018b). Investigations on air quality in the historic wooden church in Oradea city, Romania. *Environ. Eng. Manag. J. (EEMJ)* 17 (11), 2731–2739. doi:10.30638/eemj.2018.272

Ilies, D. C., Onet, A., Wendt, J. A., Ilieș, M., Timar, A., Ilies, A., et al. (2018a). Study on microbial and fungal contamination of air and wooden surfaces inside of a historical Church from Romania. *J. Environ. Biol.* 39, 980–984. doi:10.22438/jeb/39/6/MRN-658

Indrie, L., Oana, D., Ilies, M., Ilies, D. C., Lincu, A., Ilies, A., et al. (2019). Indoor air quality of museums and conservation of textiles art works. *Case study salacea Mus. House, Rom. Ind. Textila* 70, 88–93. doi:10.35530/IT.070.01.1608

Ion, R. M., Doncea, S. M., and Țurcanu-Caruțiu, D. (2018). *Nanotechnologies in cultural heritage-Materials and instruments for diagnosis and treatment*. London, UK: Novel Nanomaterials; IntechOpen, 173–190.

Jabbar, A. H., al-Janabi, H. S. O., Hamzah, M. Q., Mezan, S. O., Tumah, A. N., Ameruddin, A. S. B., et al. (2020). Green synthesis and characterization of silver nanoparticle (AgNPs) using pandanus atrocarpus extract. *Int. J. Adv. Sci. Technol.* 29, 4913–4922.

Jia, M., Zhang, X., Weng, J., Zhang, J., and Zhang, M. (2019). Protective coating of paper works: zno/cellulose nanocrystal composites and analytical characterization. *J. Cult. Herit.* 38, 64–74. doi:10.1016/j.culher.2019.02.006

Kasemets, K., Ivask, A., Dubourguier, H.-C., and Kahru, A. (2009). Toxicity of nanoparticles of ZnO, CuO and TiO2 to yeast *Saccharomyces cerevisiae*. *Toxicol. Vitro* 23, 1116–1122. doi:10.1016/j.tiv.2009.05.015

Khademi-Azandehi, P., and Moghaddam, J. (2015). Green synthesis, characterization and physiological stability of gold nanoparticles from *Stachys lavandulifolia* Vahl extract. *Particuology* 19, 22–26. doi:10.1016/j.partic.2014.04.007

Khadiran, T., Jasmani, L., and Rusli, R. (2022). "Application of nanomaterials for wood protection," in *Emerging nanimaterials: Opportunities and challenges in forestry sectors* (Cham: Springer International Publishing), 179–196.

Kumari, M., Giri, V. P., Pandey, S., Kumar, M., Katiyar, R., Nautiyal, C. S., et al. (2019). An insight into the mechanism of antifungal activity of biogenic nanoparticles than their chemical counterparts. *Pesticide Biochem. Physiology* 157, 45–52. doi:10.1016/j.pestbp.2019.03.005

Lallo da Silva, B., Caetano, B. L., Chiari-Andréo, B. G., Pietro, R. C. L. R., and Chiavacci, L. A. (2019). Increased antibacterial activity of ZnO nanoparticles: influence of size and surface modification. *Colloids Surfaces B Biointerfaces* 177, 440–447. doi:10.1016/j.colsurfb.2019.02.013

Le, A.-T., Le, T. T., Nguyen, Q., Tran, H. H., Dang, D. A., Tran, Q. H., et al. (2012). Powerful colloidal silver nanoparticles for the prevention of gastrointestinal bacterial infections. *Adv. Nat. Sci. Nanosci. Nanotechnol.* 3, 045007. doi:10.1088/2043-6262/3/4/045007

Li, X., Xu, H., Chen, Z.-S., and Chen, G. (2011). Biosynthesis of nanoparticles by microorganisms and their applications. *J. Nanomater.* 2011, 1–16. doi:10.1155/2011/270974

Lopez-Lima, D., Mtz-Enriquez, A. I., Carrión, G., Basurto-Cereceda, S., and Pariona, N. (2021). The bifunctional role of copper nanoparticles in tomato: effective treatment for Fusarium wilt and plant growth promoter. *Sci. Hortic.* 277, 109810. doi:10.1016/j.scienta.2020.109810

Lupan, I., Ianc, M. B., Kelemen, B. S., Carpa, R., Rosca-Casian, O., Chiriac, M. T., et al. (2014). New and old microbial communities colonizing a seventeenth-century wooden church. *Folia Microbiol.* 59, 45–51. doi:10.1007/s12223-013-0265-3

Maqbool, Q., Czerwinska, N., Giosue, C., Sabbatini, S., Ruello, M. L., and Tittarelli, F. (2022). New waste-derived TiO2 nanoparticles as a potential photocatalytic additive for lime based indoor finishings. *J. Clean. Prod.* 373, 133853. doi:10.1016/j.jclepro.2022.133853

Marcu, F., Hodor, N., Indrie, L., Dejeu, P., Ilieș, M., Albu, A., et al. (2021). Microbiological, health and comfort aspects of indoor air quality in a Romanian historical wooden church. *Int. J. Environ. Res. Public Health* 18 (18), 9908. doi:10.3390/ijerph18189908

Meghana, S., Kabra, P., Chakraborty, S., and Padmavathy, N. (2015). Understanding the pathway of antibacterial activity of copper oxide nanoparticles. *RSC Adv.* 5, 12293–12299. doi:10.1039/C4RA12163E

Motelica, L., Ficai, D., Oprea, O.-C., Ficai, A., Ene, V.-L., Vasile, B.-S., et al. (2021). Antibacterial biodegradable films based on alginate with silver nanoparticles and lemongrass essential oil–innovative packaging for cheese. *Nanomaterials* 11, 2377. doi:10.3390/nano11092377

Mourdikoudis, S., Pallares, R. M., and Thanh, N. T. (2018). Characterization techniques for nanoparticles: comparison and complementarity upon studying nanoparticle properties. *Nanoscale* 10 (27), 12871–12934. doi:10.1039/c8nr02278j

Moya, R., Berrocal, A., Rodriguez-Zuñiga, A., Vega-Baudrit, J., and Noguera, S. C. (2014). Effect of silver nanoparticles on white-rot wood decay and some physical properties of three tropical wood species. *Wood Fiber Sci.* 46, 527–538.

Mukherjee, P., Senapati, S., Mandal, D., Ahmad, A., Khan, M. I., Kumar, R., et al. (2002). Extracellular synthesis of gold nanoparticles by the fungus *Fusarium oxysporum*. *ChemBioChem* 3, 461. doi:10.1002/1439-7633(20020503)3:5<461::aid-cbic461>3.0.co;2-x

Nair, R. R., Demarche, P., and Agathos, S. N. (2013). Formulation and characterization of an immobilized laccase biocatalyst and its application to eliminate organic micropollutants in wastewater. *N. Biotechnol.* 30, 814–823. doi:10.1016/j.nbt.2012.12.004

Nair, S., K S, S., and R, S. (2022). "Advancements in nanotechnological applications for wood protection," in *Science of wood degradation and its protection*. Editor R. Sundararaj (Singapore: Springer).

Neamtu, C., Bratu, I., Măruțoiu, C., Măruțoiu, V. C., Nemeș, O. F., Comes, R., et al. (2021). Component materials, 3D digital restoration, and documentation of the imperial gates from the wooden church of voivodeni, sălaj county, Romania. *Appl. Sci.* 11, 3422. doi:10.3390/app11083422

Nisar, P., Ali, N., Rahman, L., Ali, M., and Shinwari, Z. K. (2019). Antimicrobial activities of biologically synthesized metal nanoparticles: an insight into the mechanism of action. *J. Biol. Inorg. Chem.* 24, 929–941. doi:10.1007/s00775-019-01717-7

Nongbet, A., Mishra, A. K., Mohanta, Y. K., Mahanta, S., Ray, M. K., Khan, M., et al. (2022). Nanofertilizers: A smart and sustainable attribute to modern agriculture. *Plants* 11, 2587. doi:10.3390/plants11192587

Ogar, A., Tylko, G., and Turnau, K. (2015). Antifungal properties of silver nanoparticles against indoor mould growth. *Sci. Total Environ.* 521 (522), 305–314. doi:10.1016/j.scitotenv.2015.03.101

Onet, A., Ilieș, D. C., Ilieș, A., Herman, G. V., Burta, L., Marcu, F., et al. (2020). Indoor air quality assessment and its perception. *Case study Hist. wooden church, Rom. Rom. Biotechnol. Lett.* 25, 1547–1553. doi:10.25083/rbl/25.3/1547.1553

Panda, S. K., Chakraborti, S., and Basu, R. N. (2018). Size and shape dependences of the colloidal silver nanoparticles on the light sources in photo-mediated citrate reduction technique. *Bull. Mater Sci.* 41, 90. doi:10.1007/s12034-018-1609-z

Paramo, L. A., Feregrino-Pérez, A. A., Guevara, R., Mendoza, S., and Esquivel, K. (2020). Nanoparticles in agroindustry: applications, toxicity, challenges, and trends. *Nanomaterials* 10, 1654. doi:10.3390/nano10091654

Pereira, L., Dias, N., Carvalho, J., Fernandes, S., Santos, C., and Lima, N. (2014). Synthesis, characterization and antifungal activity of chemically and fungal-produced silver nanoparticles against Trichophyton rubrum. *J. Appl. Microbiol.* 117, 1601–1613. doi:10.1111/jam.12652

Pietrzak, K., Otlewska, A., Puchalski, M., Gutarowska, B., and Patricia, G. (2016). Antimicrobial properties of silver nanoparticles against biofilm formation by *Pseudomonas aeruginosa* on archaeological textiles. *Appl. Environ. Biotechnol.* 1, 1. doi:10.18063/AEB.2016.02.001

Pinna, D., Galeotti, M., Perito, B., Daly, G., and Salvadori, B. (2018). *In situ* long-term monitoring of recolonization by fungi and lichens after innovative and traditional conservative treatments of archaeological stones in Fiesole (Italy. Int. Biodeterior. *Biodegr.* 132, 49–58. doi:10.1016/j.ibiod.2018.05.003

Pyzik, A., Ciuchcinski, K., Dziurzynski, M., and Dziewit, L. (2021). The bad and the good-microorganisms in cultural heritage environments-an update on biodeterioration and biotreatment approaches. *Mater. Basel* 14 (1), 177. doi:10.3390/ma14010177

Rai, M. k., Deshmukh, S. d., Ingle, A. p., and Gade, A. k. (2012). Silver nanoparticles: the powerful nanoweapon against multidrug-resistant bacteria. *J. Appl. Microbiol.* 112, 841–852. doi:10.1111/j.1365-2672.2012.05253.x

Reves-Estebanez, M., Ortega-Morales, B., Chan-Bacab, M., Granados-Echegoyen, C., Camacho-Chab, J. C., Sacarias, J. E. P., et al. (2018). Antimicrobial engineered nanoparticles in the built cultural heritage context and their ecotoxicological impact on animals and plants: a brief review. *Herit. Sci.* 6 (52), 52. doi:10.1186/s40494-018-0219-9

Rinna, A., Magdolenova, Z., Hudecova, A., Kruszewski, M., Refsnes, M., and Dusinska, M. (2015). Effect of silver nanoparticles on mitogen-activated protein kinases activation: role of reactive oxygen species and implication in DNA damage. *Mutagenesis* 30, 59–66. doi:10.1093/mutage/geu057

Rispoli, F., Angelov, A., Badia, D., Kumar, A., Seal, S., and Shah, V. (2010). Understanding the toxicity of aggregated zero valent copper nanoparticles against *Escherichia coli*. *J. Hazard. Mater.* 180, 212–216. doi:10.1016/j.jhazmat.2010.04.016

Roveri, M., Raneri, S., Bianchi, S., Gherardi, F., Castelvetro, V., and Toniolo, L. (2018). Electrokinetic characterization of natural stones coated with nanocomposites for the protection of cultural heritage. *Appl. Sci.* 8, 1694. doi:10.3390/app8091694

Ruparelia, J. P., Chatterjee, A. K., Duttagupta, S. P., and Mukherji, S. (2008). Strain specificity in antimicrobial activity of silver and copper nanoparticles. *Acta Biomater.* 4, 707–716. doi:10.1016/j.actbio.2007.11.006

Schifano, E., Cavallini, D., De Bellis, G., Bracciale, M. P., Felici, A. C., Santarelli, M. L., et al. (2020). Antibacterial effect of zinc oxide-based nanomaterials on environmental biodeteriogens affecting historical buildings. *Nanomaterials* 10, 335. doi:10.3390/nano10020335

Shantkriti, P. (2014). Rani Biological synthesis of Copper nanoparticles using Pseudomonas fluorescens. *Int. J. Curr. Microbiol. App. Sci.* 3 (9), 374–383.

Shiny, K. S., Sundararaj, R., Mamatha, N., Lingappa, B., Shiny, K. S., Sundararaj, R., et al. (2019). A new approach to wood protection: preliminary study of biologically synthesized copper oxide nanoparticle formulation as an environmental friendly wood protectant against decay fungi and termites. *Maderas. Cienc. Tecnol.* 21, 0–356. doi:10.4067/S0718-221X2019005000307

Sidorowicz, A., Fais, G., Casula, M., Borselli, M., Giannaccare, G., Locci, A. M., et al. (2023). Nanoparticles from microalgae and their biomedical applications. *Mar. Drugs* 21, 352. doi:10.3390/md21060352

Sidorowicz, A., Margarita, V., Fais, G., Pantaleo, A., Manca, A., Concas, A., et al. (2022). Characterization of nanomaterials synthesized from Spirulina platensis extract and their potential antifungal activity. *PLOS ONE* 17, e0274753. doi:10.1371/journal.pone.0274753

Slavin, Y. N., Asnis, J., Häfeli, U. O., and Bach, H. (2017). Metal nanoparticles: understanding the mechanisms behind antibacterial activity. *J. Nanobiotechnology* 15, 65. doi:10.1186/s12951-017-0308-z

Sterflinger, K., and Piñar, G. (2013). Microbial deterioration of cultural heritage and works of art — tilting at windmills? *Appl. Microbiol. Biotechnol.* 97, 9637–9646. doi:10.1007/s00253-013-5283-1

Sterflinger, K., and Pinzari, F. (2012). The revenge of time: fungal deterioration of cultural heritage with particular reference to books, paper and parchment. *Environ. Microbiol.* 14, 559–566. doi:10.1111/j.1462-2920.2011.02584.x

Stuart, B. H. (2004). *Infrared spectroscopy: Fundamentals and applications*. New York: John Wiley and Sons.

Tan, Y. N., Lee, K. H., and Su, X. (2011). Study of single-stranded DNA binding protein–nucleic acids interactions using unmodified gold nanoparticles and its application for detection of single nucleotide polymorphisms. *Anal. Chem.* 83, 4251–4257. doi:10.1021/ac200525a

Tang, S., and Zheng, J. (2018). Antibacterial activity of silver nanoparticles: structural effects. *Adv. Healthc. Mater.* 7, 1701503. doi:10.1002/adhm.201701503

Tayel, A. A., El-Tras, W. F., Moussa, S., El-Baz, A. F., Mahrous, H., Salem, M. F., et al. (2011). Antibacterial action of zinc oxide nanoparticles against foodborne pathogens. *J. Food Saf.* 31, 211–218. doi:10.1111/j.1745-4565.2010.00287.x

Xie, Y., He, Y., Irwin, P. L., Jin, T., and Shi, X. (2011). Antibacterial activity and mechanism of action of zinc oxide nanoparticles against Campylobacter jejuni. *Appl. Environ. Microbiol.* 77, 2325–2331. doi:10.1128/AEM.02149-10

Ying, S., Guan, Z., Ofoegbu, P. C., Clubb, P., Rico, C., He, F., et al. (2022). Green synthesis of nanoparticles: current developments and limitations. *Environ. Technol. Innovation* 26, 102336. doi:10.1016/j.eti.2022.102336

Zhang, L., Jiang, Y., Ding, Y., Povey, M., and York, D. (2007). Investigation into the antibacterial behaviour of suspensions of ZnO nanoparticles (ZnO nanofluids). *J. Nanopart Res.* 9, 479–489. doi:10.1007/s11051-006-9150-1

Zhang, X.-F., Liu, Z.-G., Shen, W., and Gurunathan, S. (2016). Silver nanoparticles: synthesis, characterization, properties, applications, and therapeutic approaches. *Int. J. Mol. Sci.* 17, 1534. doi:10.3390/ijms17091534